

This is a repository copy of *The Characteristics and Biological Relevance of Inorganic Amorphous Calcium Carbonate (ACC) Precipitated from Seawater*.

White Rose Research Online URL for this paper:  
<https://eprints.whiterose.ac.uk/148367/>

Version: Accepted Version

---

**Article:**

Evans, David, Webb, Paul B., Penkman, Kirsty [orcid.org/0000-0002-6226-9799](https://orcid.org/0000-0002-6226-9799) et al. (2 more authors) (2019) The Characteristics and Biological Relevance of Inorganic Amorphous Calcium Carbonate (ACC) Precipitated from Seawater. CRYSTAL GROWTH DESIGN. ISSN 1528-7483

<https://doi.org/10.1021/acs.cgd.9b00003>

---

**Reuse**

Items deposited in White Rose Research Online are protected by copyright, with all rights reserved unless indicated otherwise. They may be downloaded and/or printed for private study, or other acts as permitted by national copyright laws. The publisher or other rights holders may allow further reproduction and re-use of the full text version. This is indicated by the licence information on the White Rose Research Online record for the item.

**Takedown**

If you consider content in White Rose Research Online to be in breach of UK law, please notify us by emailing [eprints@whiterose.ac.uk](mailto:eprints@whiterose.ac.uk) including the URL of the record and the reason for the withdrawal request.

## The characteristics and biological relevance of inorganic amorphous calcium carbonate (ACC) precipitated from seawater

David Evans, Paul B. Webb, Kirsty Penkman, Roland Kröger, and Nicola Allison

*Cryst. Growth Des.*, **Just Accepted Manuscript** • DOI: 10.1021/acs.cgd.9b00003 • Publication Date (Web): 03 Jul 2019

Downloaded from [pubs.acs.org](https://pubs.acs.org) on July 9, 2019

### Just Accepted

“Just Accepted” manuscripts have been peer-reviewed and accepted for publication. They are posted online prior to technical editing, formatting for publication and author proofing. The American Chemical Society provides “Just Accepted” as a service to the research community to expedite the dissemination of scientific material as soon as possible after acceptance. “Just Accepted” manuscripts appear in full in PDF format accompanied by an HTML abstract. “Just Accepted” manuscripts have been fully peer reviewed, but should not be considered the official version of record. They are citable by the Digital Object Identifier (DOI®). “Just Accepted” is an optional service offered to authors. Therefore, the “Just Accepted” Web site may not include all articles that will be published in the journal. After a manuscript is technically edited and formatted, it will be removed from the “Just Accepted” Web site and published as an ASAP article. Note that technical editing may introduce minor changes to the manuscript text and/or graphics which could affect content, and all legal disclaimers and ethical guidelines that apply to the journal pertain. ACS cannot be held responsible for errors or consequences arising from the use of information contained in these “Just Accepted” manuscripts.

# The characteristics and biological relevance of inorganic amorphous calcium carbonate (ACC) precipitated from seawater

David Evans<sup>1,a\*</sup>, Paul B. Webb<sup>2</sup>, Kirsty Penkman<sup>3</sup>, Roland Kröger<sup>4</sup>, and Nicola Allison<sup>1</sup>

<sup>1</sup> School of Earth and Environmental Sciences, University of St Andrews, St Andrews, UK

<sup>2</sup> School of Chemistry, University of St Andrews, St Andrews, UK

<sup>3</sup> BioArCh, Department of Chemistry, University of York, York, UK

<sup>4</sup> Department of Physics, University of York, York, UK

<sup>a</sup> Now at: Institute for Geosciences, Goethe University Frankfurt, 60438 Frankfurt am Main, Germany

\*evans@em.uni-frankfurt.de

## Abstract

The importance of amorphous calcium carbonate (ACC) as a potential precursor phase in the biomineralization of marine calcifiers is increasingly being reported, particularly as the presence of ACC has been observed or inferred in several major groups. Here, we investigate the structure and conditions required to precipitate ACC from seawater-based solutions, with emphasis on the co-influence of the carbonate system (pH, dissolved inorganic carbon (DIC) concentration), seawater Mg/Ca ratio and the presence of amino acids. We find that Mg<sup>2+</sup> and the presence of aspartic acid, glutamic acid, and glycine strongly inhibit ACC precipitation. Moreover, we were unable to precipitate ACC from seawater with a carbonate chemistry within the range of that thought to characterise the calcification site of certain marine calcifiers (i.e. DIC <6 mM, pH <9.3), although substantial modification of the seawater Mg/Ca ratio (Mg/Ca<sub>sw</sub>) allowed precipitation at a reduced DIC, with the implication that this could be an important component of utilising an ACC pathway. Finally, the degree to which Mg/Ca<sub>sw</sub> and the addition of amino acids influence the structure of ACC and the necessary seawater [CO<sub>3</sub><sup>2-</sup>] for precipitation is strongly pH dependent. At lower, more biologically relevant pH than that typical of much inorganic work, decreasing Mg/Ca<sub>sw</sub> can result in greater long-range order and less water of crystallisation, but facilitates precipitation at a considerably lower [CO<sub>3</sub><sup>2-</sup>] than at higher pH.

## 1. Introduction

Amorphous calcium carbonate (ACC) has been shown to play an integral role in the biomineralisation process in a wide range of organisms,<sup>1-4</sup> including having been identified or inferred in a wide range of marine organisms including sponges,<sup>5</sup> sea urchin larvae,<sup>6</sup> ascidians,<sup>7</sup> molluscs,<sup>8</sup> coccolithophores,<sup>9</sup> corals,<sup>10</sup> and foraminifera.<sup>11-13</sup> Improving our knowledge of the role of ACC in biomineralization is important because the shells of such organisms represent one of the largest long-term sinks of carbon on Earth,<sup>14</sup> yet the effect of climate change and ocean acidification on the calcification process is not well-constrained,<sup>15</sup> in part because some key aspects are poorly understood.

1  
2  
3 Inorganic ACC precipitation work has demonstrated that  $Mg^{2+}$  and organic molecules such as  
4 phosphoamino acids play a stabilising role,<sup>5,16,17</sup> retarding the transformation of ACC into a crystalline  
5 carbonate. In addition, ACC may be stabilised in confinement,<sup>18</sup> and the crystalline  $CaCO_3$  polymorph  
6 that results from ACC depends on solution chemistry.<sup>19,20</sup> Especially relevant to this study is the  
7 identification of synthesis-dependent structural variations in inorganic ACC,<sup>21</sup> which has also been  
8 observed in biogenic samples. For example, Extended X-Ray Absorption Fine Structure (EXAFS)  
9 spectra of ACCs of different origin<sup>22</sup> demonstrates not just variable Ca-O bond distances but also  
10 variable coordination numbers around Ca.  
11  
12  
13  
14  
15

16  
17 These studies yield insights into the diversity of ACC and controls on nucleation, growth and  
18 transformation, yet most inorganic precipitation work has utilised fluid chemistries which are very  
19 different from those inferred to be present at the site of ACC formation in marine calcifiers. For  
20 example, tropical zooxanthellate corals and hyaline foraminifera calcify from a seawater-like  
21 solution,<sup>11,23–26</sup> albeit modified with respect to pH and DIC<sup>23,26–28</sup>, whilst an ongoing debate surrounds  
22 the role of pumping protons,  $Ca^{2+}$ , and  $Mg^{2+}$  into and out of the calcifying space.<sup>13,29–31</sup> In contrast,  
23 inorganic ACC is often experimentally precipitated through the decomposition of  $(NH_4)_2CO_3$  in  $CaCl_2$   
24 solutions (Ref. 32 and references therein), or by mixing relatively concentrated equimolar  $CaCl_2$  and  
25  $Na_2CO_3$  solutions.<sup>20,33,34</sup> Both techniques result in solution carbonate chemistries that are highly  
26 variable throughout the course of the experiment, and far more saturated with respect to carbonate  
27 minerals compared to the calcifying space of marine organisms. For example, the calcifying space of  
28 corals is characterised by a DIC and pH of 2–6 mM and  $<9.3$ , respectively,<sup>26,28,35,36</sup> a DIC  
29 concentration around two orders of magnitude lower than the initial solutions of e.g. Ref. 20.  
30 Furthermore, much previous ACC work was conducted in ionically simple solutions, raising the  
31 possibility that they might differ structurally and/or compositionally from biogenic ACCs. We stress  
32 that this is not intended as criticism of the large body of important work that exists, but rather  
33 highlights the need to build on these studies through the precipitation and study of ACC under  
34 conditions closer to those found in marine calcifiers.  
35  
36  
37  
38  
39  
40  
41  
42  
43  
44  
45

46  
47 We present data from a series of ACC precipitation experiments conducted in seawater-based  
48 solutions. Solution pH, DIC,  $[Mg^{2+}]$ , and  $[Ca^{2+}]$  were varied to identify how these parameters affect  
49 the fluid saturation state required for ACC precipitation from seawater. We also studied the effect of  
50 aspartic and glutamic acid because the acidic amino acids are known to form ligands with  $Mg^{2+}$  and  
51  $Ca^{2+}$  in solution,<sup>37</sup> and therefore may inhibit precipitation, as well as glycine for comparison. X-ray  
52 diffraction (XRD), Raman spectroscopy, attenuated total reflectance Fourier transform infrared  
53 spectroscopy (ATR-FTIR), and thermogravimetric analysis with coupled mass spectrometry (TGA-  
54 MS) were used to determine possible structural variations in the ACCs precipitated under different  
55 conditions.  
56  
57  
58  
59  
60

## 2. Experimental

Sixty-six precipitation experiments were conducted spanning seawater Mg/Ca ratios of 0-5 mol mol<sup>-1</sup> (achieved by varying both Mg<sup>2+</sup> and Ca<sup>2+</sup>), DIC concentrations of 3-25 mM, pH 8.9-10.3, as well as a range of L-aspartic acid, L-glutamic acid, and glycine (L-Asp, L-Glu, Gly) concentrations, and titration rates (see Tab. 1 and the Supplementary Information). We identified the solution saturation state required to precipitate ACC under these conditions, hereafter abbreviated to ACC<sub>SI</sub> (Saturation Index):

$$\text{ACC}_{\text{SI}} = [\text{Ca}^{2+}] \cdot [\text{CO}_3^{2-}] \quad (\text{Eq. 1})$$

Where [Ca<sup>2+</sup>] and [CO<sub>3</sub><sup>2-</sup>] refer to the concentrations at the onset of ACC precipitation. ACC<sub>SI</sub> is directly proportional to the CaCO<sub>3</sub> saturation state of the solution ( $\Omega$ ), where for example  $\Omega_{\text{calcite}} = [\text{Ca}^{2+}] \cdot [\text{CO}_3^{2-}] / K_{\text{sp}}(\text{calcite})$ . We use a simpler formulation of the solution saturation state because ACC  $K_{\text{sp}}$  is not well-known, and likely varies depending on the structure and composition of the ACC precipitated.<sup>38</sup> A higher ACC<sub>SI</sub> directly implies a higher [Ca<sup>2+</sup>] and/or [CO<sub>3</sub><sup>2-</sup>] required to precipitate ACC from seawater.

### 2.1 ACC precipitation

All precipitation experiments were conducted in artificial seawater (ASW) made using the protocol given in Ref. 39, modified to include the most widely studied trace elements in biogenic carbonates at a concentration approximately equivalent to open-ocean seawater (see the Supplementary Information). The majority of experiments were conducted in seawater with the natural Mg/Ca ratio of 5.2 mol mol<sup>-1</sup> (53.0/10.3 mM/mM) whilst a subset of 20 investigated the effect of independently varying both [Mg<sup>2+</sup>] and/or [Ca<sup>2+</sup>]. The salinity of most experiments was 35 PSU, except where the [Mg<sup>2+</sup>] or [Ca<sup>2+</sup>] was modified. Seawater with a [Mg<sup>2+</sup>] lower than natural was produced by adding lower amounts of MgCl<sub>2</sub>, such that in these experiments, salinity was proportional to [Mg<sup>2+</sup>] (33 PSU in MgCl<sub>2</sub>-free ASW). Seawater with a [Ca<sup>2+</sup>] higher than natural (>10.3 mM) was produced by spiking with CaCl<sub>2</sub>, such that salinity scaled linearly from 35 to 37 PSU in those with the highest [Ca<sup>2+</sup>] (50 mM).

To precipitate ACC, the carbonate chemistry of the seawater-based solutions was adjusted, by trial and error, to a state just below that required for ACC precipitation, i.e. ACC precipitation never occurred spontaneously but was initiated by subsequent dosing of small volumes of CaCl<sub>2</sub> and Na<sub>2</sub>CO<sub>3</sub>. The seawater pH and [Ca<sup>2+</sup>] were monitored using pH and Ca ion selective electrodes (ISE), calibrated using NIST-traceable buffer solutions and artificial seawater solutions respectively, the latter with a range of seawaters with [Ca<sup>2+</sup>] spanning 0-16 mM (determined by ICP-OES). Prior to ACC precipitation, the seawater carbonate chemistry was adjusted to the desired value by adding 1 M Na<sub>2</sub>CO<sub>3</sub> (to increase DIC) and 0.1 M NaOH or HCl to adjust pH (Fig. 1A). The initial seawater DIC was calculated as the measured DIC of the stock seawater plus the amount of Na<sub>2</sub>CO<sub>3</sub> added. Once the

1  
2  
3 desired solution chemistry was obtained, the seawater was stirred slowly for 60 s to allow the  
4 carbonate system to equilibrate. The Ca ISE was monitored to confirm that no precipitation occurred  
5 while the solution chemistry was being manipulated (Fig. 1B). ACC precipitation was then initiated  
6 by slow, controlled, simultaneous titration of 0.45 M CaCl<sub>2</sub> and Na<sub>2</sub>CO<sub>3</sub> solutions into the seawater.  
7 All precipitations were conducted in acid-cleaned (1 M HCl) High-Density Polyethylene (HDPE)  
8 beakers at 22.5±1.5°C using a Metrohm 902 Titrand titrator. The Ca<sup>2+</sup> ISE has a minor sensitivity to  
9 pH (a 1 unit pH change results in an approximate seawater [Ca<sup>2+</sup>] bias of 15%) which was corrected  
10 for using the pH electrode.  
11  
12  
13  
14  
15  
16

17 The solution chemistry ([Ca<sup>2+</sup>], pH and [DIC]) conditions at the onset of ACC precipitation were  
18 identified by comparing the observed evolution of [Ca<sup>2+</sup>] using the calibrated Ca ISE to that predicted  
19 if all titrated CaCl<sub>2</sub> remained in solution (Fig. 1B). The seawater [Ca<sup>2+</sup>] at ACC<sub>SI</sub> (the conditions at  
20 which precipitation began) is defined here as the point at which more than 20% of the titrated CaCl<sub>2</sub>  
21 was utilised in precipitation. Whilst this method slightly overestimates the solution saturation state  
22 with respect to carbonate precipitates (compare arrows 2 and 3 in Fig. 1C), this compromise was  
23 ultimately preferred over the uncertainty associated with precisely defining the point at which the Ca<sup>2+</sup>  
24 titration curve deviated from expected, as the Ca ISE has a precision of ~3% in high-ionic strength  
25 solutions such as seawater. The seawater [CO<sub>3</sub><sup>2-</sup>] required to calculate ACC<sub>SI</sub> was calculated from  
26 DIC and pH using co2sys,<sup>40</sup> based on the titration of exactly equal volumes of Na<sub>2</sub>CO<sub>3</sub> and CaCl<sub>2</sub> up  
27 until the point that precipitation began, i.e. ΔDIC = ΔCa. In these relatively short experiments  
28 (precipitation typically took place over <5 minutes, total experiment duration including seawater  
29 carbonate chemistry adjustment was <20 minutes), the seawater carbonate chemistry was assumed to  
30 be unaffected by CO<sub>2</sub> diffusion from the atmosphere.  
31  
32  
33  
34  
35  
36  
37  
38  
39  
40

41 The majority of experiments were conducted in 100-200 ml seawater, with a subset (20 precipitations)  
42 conducted in 250 ml. In these larger volume experiments seawater samples for DIC and elemental  
43 chemistry were taken, albeit only after sufficient precipitation had taken place for characterisation  
44 (30-60 s after ACC<sub>SI</sub>, the point at which precipitation began), see the Supplementary Information for  
45 further details. The seawater-precipitate mixtures were immediately vacuum separated using 0.2 μm  
46 nylon membrane filters, and the DIC of the filtrate was immediately determined. Samples for  
47 elemental analysis were placed into acid-cleaned (1 M HCl) polypropylene centrifuge tubes and  
48 immediately acidified to 5% HNO<sub>3</sub>. The precipitates were thoroughly rinsed with trace element grade  
49 ethanol and air-dried. We observe good agreement between the measured Mg/Ca and DIC estimates  
50 based on the technique outlined in the preceding paragraph (typically better than 7% in both cases, see  
51 the Supplementary Information)  
52  
53  
54  
55  
56  
57  
58  
59  
60

1  
2  
3 Based on the technique described above, we calculate the solution carbonate chemistry (pH, DIC,  
4  $[\text{CO}_3^{2-}]$ ),  $[\text{Ca}^{2+}]$  and Mg/Ca ratio at the onset of precipitation, use these data to compute  $\text{ACC}_{\text{SI}}$ , and  
5 subsequently examine how this is impacted by the experimental variables described above  
6 (summarised in Tab. 1). The seawater Mg/Ca ratio at the onset of precipitation was calculated as  
7  $[\text{Mg}^{2+}_{\text{initial}}]/([\text{Ca}^{2+}_{\text{initial}}] + \text{Ca}^{2+}_{\text{titrated}})$ , i.e. assuming the titrant solutions did not contain a significant Mg  
8 contaminant, and that only a minor amount of  $\text{Mg}^{2+}$  was removed through ACC precipitation. We  
9 estimate that precipitation of 20 mg ACC (typical of the 250 ml experiments) with a Mg concentration  
10 of 10 mole %<sup>41</sup> reduced the solution  $[\text{Mg}^{2+}]$  by 0.04 mM, or 0.4%, which we consider to be  
11 unimportant in the context of the large range investigated here (0-53 mM). Similarly, the relatively  
12 small titration volumes necessary to precipitate ACC using this method (~1-4 ml in 100-250 ml  
13 seawater) meant that there was no substantial change in ionic strength over the course of the  
14 experiments.  
15  
16  
17  
18  
19  
20  
21  
22

## 23 **2.2 Analytical chemistry**

24 The uncertainty in the measurement of pH was calculated as 0.020 across the pH range 4-10, based on  
25 the maximum observed difference between fresh and one-week-old pH buffers (the buffers used to  
26 perform the calibration were replaced approximately once per week).  
27  
28  
29  
30

31 Seawater DIC was analysed using a LI-7000  $\text{CO}_2$  differential, non-dispersive, infrared gas analyser  
32 (Apollo SciTech; AS-C3). The instrument was calibrated at intervals using a seawater standard  
33 (Dickson batch 141, DIC  $2033.3 \pm 0.3 \text{ mol kg}^{-1}$ ), and the accuracy and linearity of the analyser at the  
34 relatively high DIC concentrations of this study was confirmed by analysis of a range of  $\text{Na}_2\text{CO}_3$   
35 solutions spanning 1.5-16 mM. The precision of individual samples assessed through multiple (6-10)  
36 injections was routinely better than 0.2%. However, because the DIC analyser was not always  
37 calibrated before each set of experiments, and significant variations in the DIC calibration were  
38 observed, we report a DIC uncertainty of  $\pm 7\%$  based on the maximum difference between calibrations  
39 performed on different days.  
40  
41  
42  
43  
44  
45  
46

47  $\text{Mg}/\text{Ca}_{\text{sw}}$  was determined using the Varian Vista Pro ICP-OES (axial) at the Edinburgh Earth  
48 Observatory. The samples were diluted 1:50 with 3%  $\text{HNO}_3$  to reduce the plasma loading associated  
49 with high-ionic strength solutions. Yttrium was used as the internal standard. Calibration was  
50 performed using a six-point calibration line (blank plus five standards), spanning the range of sample  
51 Mg and Ca concentrations. Accuracy and precision (2RSD) of measured  $\text{Mg}/\text{Ca}_{\text{sw}}$  were 1.8% and  
52 2.2% respectively based on repeat analyses of natural seawater.  
53  
54  
55  
56  
57

## 58 **2.3 Precipitate characterisation**

Raman, ATR-FTIR, XRD, and TGA-MS analysis were performed on a subset of the precipitates covering the range of experimental conditions. Raman spectroscopy measurements were performed using a Horiba Jobin Yvon LabRam HR800 with a 50× long-working-distance objective, an excitation wavelength of 514 nm, and beam diameter of 1 μm. The system was calibrated prior to each set of measurements using an Ag standard. Measurements were performed at 1.8 cm<sup>-1</sup> resolution with the reported spectra representing the average of 20×5s scans. Initial measurements were performed at a low laser intensity to ensure that local heating on the sample did not alter the ACC. The laser intensity was then systematically increased to maximise signal/noise whilst ensuring no thermally induced transformation took place (i.e. no change in the spectra when normalised to the most intense peak). Subsequent full width at half maximum peak height (FWHM) analysis is dependent on spectral resolution,<sup>42,43</sup> such that the relatively wide peak widths we report for crystalline CaCO<sub>3</sub> should be viewed in the context of the spectral resolution used here. In contrast, the disordered nature of ACC means that the peaks of interest are weakly dependent on spectral resolution (>20 wavenumbers wide) and easily distinguishable from crystalline materials (~4 times wider). ATR-FTIR spectra were collected using a Bruker Platinum ATR infrared spectrometer fitted with a TGS detector; measurements were performed at 1.4 cm<sup>-1</sup> resolution with 32 scans. A baseline measurement was performed before every sample. TGA-MS profiles were determined using a Netzsch STA 449 F1 Jupiter coupled with a QMS 403 Aëolos R quadrupole mass spectrometer. Around 10 mg of sample was heated at a rate of 10°C min<sup>-1</sup> from 40°C to 800°C, in an Ar atmosphere with a flow rate of 350 ml min<sup>-1</sup>. As well as TGA profiles, the ion current of m/z 18, 28 and 44 was monitored to enable the identification of the decomposition products. In order to calculate the formula water of crystallisation, the relationship between n·H<sub>2</sub>O and the integrated area of the m/z 18 ion peak was calibrated based on the thermal decomposition of CaC<sub>2</sub>O<sub>4</sub>·H<sub>2</sub>O (see the Supplementary Information).

### 3. Results and discussion

The solution chemistry conditions at ACC<sub>SI</sub> (the onset of precipitation) is shown in pH-DIC space in Fig. 2. The majority of experiments fall within ±2 mM of the 10 mM [CO<sub>3</sub><sup>2-</sup>] line (dashed contours overlain on Fig. 2), equivalent to a [Ca<sup>2+</sup>]/[CO<sub>3</sub><sup>2-</sup>] ratio of ~1-1.2, with the exception of those in which the Mg/Ca ratio was modified. Given that the experimental seawaters did not have initial equimolar concentrations of [Ca<sup>2+</sup>] and [CO<sub>3</sub><sup>2-</sup>], this is not an artefact of the experimental design. Therefore, we find that in seawater with a Mg/Ca ratio close to natural (5 mol mol<sup>-1</sup>), ACC precipitation occurs when the DIC concentration reaches a value necessary to achieve approximately equimolar seawater [CO<sub>3</sub><sup>2-</sup>] and [Ca<sup>2+</sup>].

#### 3.1 Vibrational spectroscopy and thermal decomposition

Raman, FTIR, XRD and TGA-MS analyses (Fig. 3,4,5,6), confirm that our experiments yielded ACC in all but two cases. Experiments conducted in seawater with an initial Mg/Ca ratio <1 mol mol<sup>-1</sup>



1  
2  
3 resulted in rapid calcite precipitation without an observed ACC precursor (e.g. Fig. 3F,5), while those  
4 conducted at the highest pH (10.3 on the NBS scale) resulted in amorphous brucite-CaCO<sub>3</sub> mixtures  
5 (Fig. 4H).  
6

7  
8 In the variable pH/DIC experiments, there is no resolvable control of solution carbonate chemistry on  
9 any aspect of the Raman and FTIR spectra when precipitation takes place from normal seawater  
10 (Mg/Ca = 53/10.3 mM/mM) at pH ~10. Whilst DIC and pH were varied across a wide range, most  
11 ACCs were precipitated at a [CO<sub>3</sub><sup>2-</sup>] of 10±2 mM and a Mg/Ca<sub>sw</sub> ratio of ~5 mol mol<sup>-1</sup> (Fig. 2). This  
12 may explain why there is little evidence for a carbonate chemistry control on ACC structure, as the  
13 seawater [Ca<sup>2+</sup>]/[CO<sub>3</sub><sup>2-</sup>] ratio was close to one in most cases. Similarly, in the variable amino acid  
14 concentration experiments, we find no resolvable structural effect on ACC as evidenced by the FTIR  
15 or Raman spectra (Fig. 3 and 4), in agreement with a previous study.<sup>44</sup> These molecules have a  
16 differential affinity to form ligands with Ca<sup>2+</sup> and Mg<sup>2+</sup> in solution, such that amino acid concentration  
17 affects the free Mg/Ca ratio.<sup>37</sup> Therefore, it is somewhat surprising that the concentration of Asp and  
18 Glu do not resolvably impact ACC structure, as both influence Mg incorporation into ACC, and we  
19 identify Mg/Ca<sub>sw</sub> as a driver of ACC structure (Fig. 7).  
20  
21  
22  
23  
24  
25  
26  
27

28  
29 The Raman spectra of ACC (Fig. 3) are dominated by a broad  $\nu_1$  peak (CO<sub>3</sub> symmetric stretch) at  
30 1080 cm<sup>-1</sup> (the precise location of this peak varies as a function of mole % Mg<sup>42</sup>), and a smaller broad  
31  $\nu_4$  peak (CO<sub>3</sub> in-plane bend) at 710 cm<sup>-1</sup>. In ACC precipitated from seawater with the natural [Mg<sup>2+</sup>]  
32 and [Ca<sup>2+</sup>], the lattice mode vibrations of the crystalline CaCO<sub>3</sub> polymorphs, if present, are obscured  
33 due to the presence of a broad band below 300 cm<sup>-1</sup>. This feature occurs in both biogenic ACC<sup>2</sup> and  
34 inorganic hydrated crystalline and amorphous CaCO<sub>3</sub> (Ref. 45), but not in the crystalline anhydrous  
35 polymorphs (e.g. Fig. 3F), indicating that it relates to the presence of water. In contrast, ACC  
36 precipitated from seawater with Mg<sup>2+</sup> reduced from 53 to 10 mM (Fig. 3E) is characterised by spectra  
37 with narrower  $\nu_1$  and  $\nu_4$  peaks, as well as distinguishable lattice mode vibrations at 155 cm<sup>-1</sup> and 285  
38 cm<sup>-1</sup>, indicative of the crystal structure of calcite. These precipitates either differ structurally from  
39 their counterparts formed at higher Mg/Ca<sub>sw</sub> or represent physical mixtures of calcite and ACC.  
40 Interestingly, the Raman spectra of the precipitates presented here show many of the different features  
41 reported for both stable and transient biogenic ACCs.<sup>2</sup> Given that the differences in the Raman spectra  
42 between our experiments are principally driven by the seawater Mg/Ca ratio, this raises the possibility  
43 that variation in the structure of biogenic ACCs also arise from the Mg/Ca ratio at the site of  
44 calcification, further discussed below.  
45  
46  
47  
48  
49  
50  
51  
52  
53  
54

55  
56 The full width at half maximum (FWHM) of the symmetric C-O stretch ( $\nu_1$ ) peak at ~1080 cm<sup>-1</sup> of all  
57 ACCs is positively correlated with Mg/Ca<sub>sw</sub> and greatly exceed that of calcite and aragonite (22-34  
58 cm<sup>-1</sup> compared to 5.5-10.8 cm<sup>-1</sup> respectively, Fig. 7). Note that this comparison should be viewed in  
59 the context of the spectral resolution of our Raman data (~1.8 cm<sup>-1</sup>), such that the FWHM of the ACC  
60

1  
2  
3 samples may differ even more from calcite and aragonite than is apparent. The Root Mean Square  
4 Error (RMSE) of the  $\nu_1$  FWHM based on the data in Fig. 7 is  $1.1 \text{ cm}^{-1}$ , such that these ACCs are  
5 significantly different from the crystalline samples (as previously described<sup>4</sup>), and the relationship  
6 between  $\text{Mg}/\text{Ca}_{\text{sw}}$  and FWHM of the ACCs is highly significant ( $R^2 = 0.92$ ;  $p \ll 0.01$ ). The relatively  
7 wide ACC  $\nu_1$  peak occurs because materials lacking long-range order are typically characterised by  
8 broader peaks, in the case of ACC due to the disordered coordination environment around the Ca  
9 atoms compared to calcite.<sup>46</sup> In addition, both the relatively large  $\nu_1$  peak width in ACC and the  
10 increase in  $\nu_1$  FWHM with  $\text{Mg}/\text{Ca}_{\text{sw}}$  arise because ACC typically contains  $>10$  mole % Mg.<sup>42</sup> Because  
11 Mg-O has a longer metal-O bond distance than Ca-O, (increasing) Mg incorporation results in greater  
12 bulk heterogeneity in metal-O vibrations, and a wider  $\nu_1$  peak. In this respect, our data are in good  
13 agreement with those of Ref. 42 who found the  $\nu_1$  FWHM is linearly dependent on the mole % Mg of  
14 ACC. Whilst we cannot directly compare our results to that study as we do not report precipitate  
15 Mg/Ca data, it has been shown that ACC Mg/Ca is proportional to  $\text{Mg}/\text{Ca}_{\text{sw}}$ ,<sup>41</sup> such that our data are  
16 consistent with this finding.  
17  
18  
19  
20  
21  
22  
23  
24  
25  
26

27 Both one and two peak fits of the  $\nu_1$  band of amorphous precipitates formed under different  $\text{Mg}/\text{Ca}_{\text{sw}}$   
28 are shown in Fig. 7A. The position of the peaks in the two-peak fit were fixed at  $1080 \text{ cm}^{-1}$  and  $1090$   
29  $\text{cm}^{-1}$  ( $\text{CaCO}_3$  and  $\text{MgCO}_3$  respectively<sup>47</sup>), whilst the peak widths were fixed at  $20 \text{ cm}^{-1}$ , the intercept of  
30 our  $\text{Mg}/\text{Ca}_{\text{sw}}$ -FWHM regression (Fig. 7A), inferred to represent Mg-free ACC. A single peak fit is  
31 likely more appropriate if the  $\nu_1$  band is symmetrical and therefore explicable by solid solution of  
32 amorphous  $(\text{Ca},\text{Mg})(\text{CO}_3)_2$ , whereas a two peak fit may be more appropriate if the  $\nu_1$  band is  
33 asymmetrical, which would imply a heterogenous material. The residuals of the one and two-peak fit  
34 are similar for ACCs precipitated from different  $\text{Mg}/\text{Ca}_{\text{sw}}$  ratios achieved by varying  $\text{Ca}^{2+}$  at constant  
35  $\text{Mg}^{2+}$  (Fig. 7B-C). Therefore, the  $\nu_1$  band of these ACCs is (i) not resolvably asymmetric (cf. Ref. 42),  
36 and (ii) well-described by two closely-spaced peaks representing amorphous  $\text{CaCO}_3$  and  $\text{MgCO}_3$   
37 endmembers; a solid-solution model of Mg incorporation into ACC is compatible with these data. In  
38 contrast, ACC precipitated from seawater with a  $\text{Mg}^{2+}$  concentration reduced from 53 to 10 mM  
39 ( $\text{Mg}/\text{Ca}_{\text{sw}} = \sim 1$ ; Fig. 7D) is characterised by an asymmetrical  $\nu_1$  band, which cannot be modelled by  
40 any combination of the two-peak fit. Rather, the best-fit two-peak model arises through the  
41 combination of a relative wide peak ( $20 \text{ cm}^{-1}$ ) centred on  $1080 \text{ cm}^{-1}$  and a much narrower ( $8 \text{ cm}^{-1}$ )  
42 peak centred on  $1086 \text{ cm}^{-1}$  (this fit was determined by fixing the position and FWHM of the wider  
43 peak for the same reasons as above and solving for all other parameters, i.e. treating the second  
44 component as a complete unknown). The narrow peak indicates the presence of a more ordered phase,  
45 whilst the position of this peak is consistent with that of low-Mg calcite.<sup>47</sup> Thus, precipitation at a  
46  $[\text{Mg}^{2+}]$  greatly lower than normal seawater may result in ACC-calcite mixtures despite the overall  
47 highly saturated conditions investigated (Tab. 1). The implication of this is that within the DIC and  
48 pH range investigated here (as close as possible to that thought to characterise certain marine  
49  
50  
51  
52  
53  
54  
55  
56  
57  
58  
59  
60

1  
2  
3 calcifiers) it appears that there is a limit to which the  $[\text{Mg}^{2+}]$  can be reduced before the resulting  
4 precipitate is not entirely ACC.  
5  
6

7  
8 The most prominent feature of the FTIR spectra is the split  $\nu_3$  band at  $\sim 1400$  and  $1474\text{ cm}^{-1}$   
9 (antisymmetric  $\text{CO}_3$  stretch; Fig. 4), indicating that there is more than one local symmetry around the  
10  $\text{CO}_3$  ion in ACC,<sup>2</sup> and therefore that ACCs do have a short-range order. The broad band derived from  
11 the hydrogen-bonded O-H stretch between  $3000\text{--}3800\text{ cm}^{-1}$  indicates the presence of a significant  
12 amount of water of crystallisation, confirmed by TGA-MS (Fig. 6A). The thermal decomposition  
13 profiles of ACC precipitated from normal seawater ( $\text{Mg}/\text{Ca} = 53/10.3\text{ mM}/\text{mM}$ ) show a mass loss  
14 associated with the  $m/z$  18 ion beam of 17-19%, equivalent to a formula mass of  $\text{CaCO}_3 \cdot$   
15  $0.85 \pm 0.05\text{H}_2\text{O}$ . As in the case of the Raman and FTIR spectra, we find no systematic relationship  
16 between water content and seawater carbonate chemistry or amino acid concentration.  
17  
18  
19  
20  
21  
22

23  
24 ACC precipitated from seawater with a  $[\text{Mg}^{2+}]$  reduced to 10 mM has a narrower  $\nu_2$  peak at  $864\text{ cm}^{-1}$   
25 and a greatly reduced O-H band between  $3000\text{--}3800\text{ cm}^{-1}$  (Fig. 4F). This further indicates that the  
26  $\text{Mg}^{2+}$  concentration or ratio of  $\text{Mg}/\text{Ca}$  imparts the greatest effect on the structure of ACC and water of  
27 crystallisation (and/or results in ACC-crystalline mixtures at low  $[\text{Mg}^{2+}]$  as discussed above; Fig. 7D).  
28 Moreover, although varying pH and DIC result in no resolvable structural differences in ACC  
29 precipitated from normal seawater, we find that this is not the case as  $\text{Mg}/\text{Ca}_{\text{sw}}$  is reduced. At pH 10.1  
30 and a seawater  $\text{Mg}/\text{Ca}$  ratio of  $1\text{ mol mol}^{-1}$ , achieved by raising  $[\text{Ca}^{2+}]$  from 10 to 50 mM, the  
31 resulting ACC has an FTIR spectra equivalent to those of precipitates from seawater with the natural  
32  $\text{Mg}/\text{Ca}$  ratio (compare panels A and D in Fig. 4). However, when ACC is precipitated from seawater  
33 with 50 mM  $\text{Ca}^{2+}$  but a pH slightly reduced to 9.7, the resulting spectra are characterised by a  
34 narrower  $\nu_2$  peak at  $864\text{ cm}^{-1}$  (FWHM reduced from  $15.5$  to  $7.2\text{ cm}^{-1}$ , see Fig. 4D,E), as well as a  
35 narrower Raman  $\nu_1$  peak. The asymmetry of the  $\nu_3$  band, lack of a resolvable  $\nu_1$  peak in the FTIR  
36 spectra, and the presence of a significant amount of water of crystallisation indicate a dominantly  
37 amorphous precipitate. However, the bulk material has a greater degree of short-range order compared  
38 to ACC precipitated from normal seawater. Previous work has shown that the presence of ‘additives’  
39 like  $\text{Mg}^{2+}$  impact the short-range structure of ACC<sup>21,48</sup>; our results demonstrate that the extent to  
40 which the seawater  $\text{Mg}/\text{Ca}$  ratio drives structural differences is dependent on the carbonate chemistry.  
41 Specifically, the seawater  $\text{Mg}/\text{Ca}$  ratio exerts a larger influence on the structure of these materials at  
42 lower (more biologically relevant) pH. Given that  $\text{Mg}/\text{Ca}_{\text{sw}}$  is the only investigated method by which  
43 the solution  $[\text{Ca}^{2+}]/[\text{CO}_3^{2-}]$  ratio at the onset of precipitation can be greatly reduced below unity (Fig.  
44 2), it may be that the mechanistic basis for the  $\text{Mg}/\text{Ca}_{\text{sw}}$ -dependent structural variation in ACC is  
45 rooted in precipitation from solutions with a relatively low  $[\text{CO}_3^{2-}]$ . Of relevance here is the previous  
46 use of nuclear magnetic resonance (NMR) spectroscopy to identify structural differences in the  
47 position of mobile water in biological ACC compared to synthetic ACC produced at high pH.<sup>49</sup> We  
48  
49  
50  
51  
52  
53  
54  
55  
56  
57  
58  
59  
60

find that the seawater Mg/Ca ratio is the only parameter we varied that resulted in a substantial variation in the precipitate water of crystallisation (Fig. 4). Together, these observations again point to Mg/Ca<sub>sw</sub> as a key factor that could result in structural differences in both the precipitates discussed here as well as biogenic ACCs.

### 3.2 Solution chemistry control on ACC precipitation from seawater

The impacts of the investigated variables on ACC<sub>SI</sub> (Eq. 1) are summarised in Fig. 8 and 9. Because some factors unavoidably covaried in our experiments (especially solution [Ca<sup>2+</sup>] with other variables), the experiments were grouped into five broad sets on which to perform least-squares multiple linear regression analyses (Tab. 2). The aim of this exercise was to identify which factors (the carbonate system, solution [Mg<sup>2+</sup>] and/or [Ca<sup>2+</sup>], and amino acid concentration) exert the largest control on ACC<sub>SI</sub> where these vary together, and to explore how much of the variance in the data can be explained by these variables alone. A linear model of the following form was chosen for simplicity:

$$\text{ACC}_{\text{SI}} = x_1 + x_2 \text{Mg/Ca}_{\text{sw}} + x_3 \text{pH} + x_4 \text{DIC} + x_5 [\text{AA}] \quad (\text{Eq. 2})$$

However, we note that there is no theoretical basis for this, and more complex models could result in better fits to the data if ACC<sub>SI</sub> is nonlinearly sensitive to some factors. pH and DIC were used to account for the carbonate system because these were the variables that were measured, but ACC<sub>SI</sub> may be mechanistically more appropriately related to (e.g.) pH and [CO<sub>3</sub><sup>2-</sup>] (albeit there is no significant difference in the model fits if [CO<sub>3</sub><sup>2-</sup>] rather than DIC is chosen).

All multiple linear regression models are highly significant (Tab. 2, p << 0.01), except for the glutamic acid experiment which contained far fewer precipitations. This exercise demonstrates that solution pH, DIC, [Mg<sup>2+</sup>], [Ca<sup>2+</sup>], and amino acid concentration can explain nearly all the variance in the data (model R<sup>2</sup> range between 0.79-0.98, RMSE 5.2-9.3). Grouping all data together results in a model in which all independent variables except for amino acid concentration are significant predictors of ACC<sub>SI</sub>, with ACC<sub>SI</sub> being most sensitive to pH (m = ~50 per unit), followed by Mg/Ca<sub>sw</sub> (m = ~30 per mol/mol).

The relationship between DIC and ACC<sub>SI</sub> is not significant when DIC alone is considered (Fig. 8A), yet the multiple linear regression models demonstrate that in the amino acid-free experiments DIC is a significant predictor of ACC<sub>SI</sub> both at normal and low seawater Mg concentrations, and when the entire dataset is combined (Tab. 2). This relationship is significant irrespective of whether our best estimate of ACC<sub>SI</sub> is used, or if the uncertainty in ACC<sub>SI</sub> (mostly derived from the DIC calibration) is fully propagated through to the model by Monte Carlo simulation (1000 simulations per model, see the SI for details), because almost all of the uncertainty in ACC<sub>SI</sub> is derived from the DIC uncertainty (the uncertainties are almost perfectly correlated). As a result, the uncertainty in absolute DIC has a

1  
2  
3 very minor effect on the multiple linear regression models, and we are therefore able to identify the  
4 carbonate system as a significant factor influencing ACC precipitation from seawater. Specifically,  
5 increasing DIC and/or pH increases  $ACC_{SI}$ . All else being equal this would imply a higher  $[CO_3^{2-}]$   
6 necessary for ACC precipitation, which indicates that some factor slightly inhibits precipitation under  
7 these overall more saturated conditions. Potentially relevant considerations are pH or concentration-  
8 dependent ion-pairing, or the size of hydration spheres.  
9  
10  
11  
12

13  
14 Titration rate was not found to impart a systematic control on  $ACC_{SI}$  (Fig. 8D), and this factor was not  
15 investigated further. Importantly, however, this result does indicate that varying titration rate by more  
16 than an order of magnitude does not greatly affect the identification of  $ACC_{SI}$  using this experimental  
17 design.  
18  
19  
20

21  
22 High concentrations of the acidic amino acids substantially inhibit ACC precipitation (Fig. 8E,F), so it  
23 is surprising that the  $ACC_{SI}$  slope associated with this factor in the multiple linear regression models  
24 is relatively minor ( $m = 0.1-0.6$  per mM; Tab. 2). The reason for this may be that the inhibitory effect  
25 of amino acids in seawater is principally overcome through the addition of  $Ca^{2+}$  in our experiments  
26 (Fig. 1C), so that  $ACC_{SI}$  is ultimately best correlated with the seawater Mg/Ca ratio. To test this, the  
27 linear regression models were run both with and without amino acid concentration as an independent  
28 variable (Tab. 2). In the amino-acid free models Mg/ $Ca_{sw}$  becomes a significant predictor of  $ACC_{SI}$ ,  
29 which is to be expected in the case of collinearity in the independent variables, adding support to the  
30 above hypothesis. That is, the non-significance of Mg/ $Ca_{sw}$  as a predictor of  $ACC_{SI}$  in the amino acid  
31 experiments when both [AA] and Mg/ $Ca_{sw}$  are used in the regression model results from the tight  
32 correlation between [AA] and Mg/ $Ca_{sw}$  at the onset of precipitation, as the inhibitory effects of the  
33 amino acids is overcome through the additional titration of  $Ca^{2+}$ .  
34  
35  
36  
37  
38  
39  
40  
41

42  
43 The role of  $Mg^{2+}$  in both inhibiting ACC precipitation and stabilising against transformation to a  
44 crystalline  $CaCO_3$  is well-known.<sup>2,50,51</sup> It is therefore unsurprising that we find it also plays a similarly  
45 important role in ACC precipitation from seawater. Reducing seawater  $[Mg^{2+}]$  from 53 to 10 mM  
46 enables precipitation at a moderately lower  $ACC_{SI}$ , and therefore a lower DIC, given the initial  
47 seawater  $[Ca^{2+}]$  was not varied in these experiments (Fig. 8B). By conducting a set of experiments at  
48 different pH and DIC with  $[Mg^{2+}]$  reduced to 10 mM, we show that it is possible to precipitate ACC at  
49 a DIC below 10 mM (Fig. 8B,C), i.e. approaching those conditions thought to characterise marine  
50 calcifiers, discussed in more detail below. However, the resulting lower  $Mg^{2+}$  concentration of the  
51 seawater, and therefore the ACC precipitates,<sup>41</sup> has been shown to reduce the time required for this  
52 ACC to transform into calcite or monohydrocalcite,<sup>51</sup> with the implication that although the DIC  
53 required to precipitate ACC is greatly reduced, the resulting ACC is likely less stable. Indeed, large  
54  
55  
56  
57  
58  
59  
60

1  
2  
3 structural differences between ACC from normal and low-Mg seawater were observed as discussed in  
4 Sec. 3.1.  
5  
6

7  
8 In contrast to the effect of reducing  $[\text{Mg}^{2+}]$ , decreasing  $\text{Mg}/\text{Ca}_{\text{sw}}$  by elevating seawater  $[\text{Ca}^{2+}]$  at pH 10  
9 results in a higher  $\text{ACC}_{\text{SI}}$  (Fig. 8B). This is borne out by the experimental data overall, which broadly  
10 fall on a  $\text{Mg}/\text{Ca}_{\text{sw}}-\text{ACC}_{\text{SI}}$  array characterised by a negative slope (Fig. 9A, Tab. 2), which means that  
11 increasing  $\text{Ca}^{2+}$  does not result in a proportionally equivalent  $\text{CO}_3^{2-}$  decrease to maintain a constant  
12 solution  $[\text{Ca}^{2+}]\cdot[\text{CO}_3^{2-}]$  (the definition of  $\text{ACC}_{\text{SI}}$ ). Nonetheless, although a higher  $[\text{Ca}^{2+}]$  results in a  
13 higher  $\text{ACC}_{\text{SI}}$ , precipitation is possible at a lower DIC and  $[\text{CO}_3^{2-}]$  compared to normal seawater (Fig.  
14 8B), as in the case when  $\text{Mg}/\text{Ca}_{\text{sw}}$  is reduced by lowering  $[\text{Mg}^{2+}]$ . Moreover, performing a similar  
15 experiment at a lower pH of 9.5 highlights the importance of considering seawater elemental and  
16 carbonate chemistry in tandem. In contrast to the experiments at pH 10, increasing  $[\text{Ca}^{2+}]$  at pH 9.5  
17 yields precipitation at an approximately constant  $\text{ACC}_{\text{SI}}$  (Fig. 8B) and even lower DIC. The  
18 implication of this is that seawater chemistry exerts a bigger influence on the dynamics of ACC  
19 precipitation at lower pH, in addition to the wider structural variation in ACC precipitated at lower pH  
20 discussed above (Fig. 4).  
21  
22  
23  
24  
25  
26  
27  
28  
29

30 In summary, we find that reducing  $\text{Mg}/\text{Ca}_{\text{sw}}$ , either by raising  $\text{Ca}^{2+}$  or lowering  $\text{Mg}^{2+}$  is the principal  
31 means by which ACC precipitation may be formed from seawater with a relatively low DIC. We  
32 stress that additional considerations like the carbonate system,<sup>52,53</sup> and moreover the possible presence  
33 of a variety of organic molecules,<sup>7,17,54</sup> and/or confinement<sup>18</sup> may provide additional mechanisms by  
34 which ACC can be synthesised and stabilised, potentially independently of solution major ion  
35 chemistry. However, our results demonstrate that the concentration of both  $\text{Mg}^{2+}$  and  $\text{Ca}^{2+}$  are  
36 important in determining the precipitation and structure of ACC, and that precipitation and structure  
37 are more sensitive to solution ion chemistry at lower pH. Lastly, we find that the presence of Mg in  
38 seawater is critical to ACC precipitation. None of our experiments in Mg-free ASW yielded ACC,  
39 instead resulting in rapidly-precipitated calcite (Figs. 3F,5).  
40  
41  
42  
43  
44  
45  
46

47 ACC precipitation at different amino acid concentrations demonstrates that the presence of all three  
48 amino acids increase  $\text{ACC}_{\text{SI}}$ . As is the case for crystalline  $\text{CaCO}_3$ ,<sup>55</sup> the effect of the acidic amino  
49 acids is distinct from glycine. Specifically, we find that  $[\text{Gly}]$  exerts a relatively minor, approximately  
50 linear, control on  $\text{ACC}_{\text{SI}}$ , whilst the effect of increasing  $[\text{Asp}]$  or  $[\text{Glu}]$  is both more pronounced and  
51 nonlinear (Fig. 8E). Relatively low concentrations of both these acidic amino acids result in an  
52 increase in  $\text{ACC}_{\text{SI}}$  from  $\sim 150$  to 200, i.e. greater than the change affected by the entire studied range  
53 of pH and DIC. Above an amino acid concentration of 20 mM there is little further effect, indicating  
54 that the inhibition of ACC precipitation by Asp and Glu becomes saturated above this point. As in the  
55  
56  
57  
58  
59  
60

1  
2  
3 case of  $\text{Mg}^{2+}$ , our results show that the amino acids, as well as playing a stabilising role,<sup>47</sup> also serve  
4 to inhibit ACC precipitation.  
5  
6

7  
8 Varying the seawater carbonate system in the presence of 50 mM Asp and three different [Gly] (Fig.  
9 8F) again highlights the importance of considering all aspects of solution chemistry when studying  
10 ACC precipitation. For example, at the lower range of [Gly] studied here (2 mM),  $\text{ACC}_{\text{SI}}$  falls on the  
11 amino acid-free variable pH/DIC array (Fig. 8F). However, at an [Asp] or [Gly] of 50 mM, the data  
12 fall above the array, as the presence of high concentrations of amino acids inhibits ACC precipitation,  
13 but crucially, the degree to which this is the case strongly depends on the seawater carbonate  
14 chemistry. At the lower pH range investigated here ( $\sim 9$ ), the inhibitory effect on ACC precipitation is  
15 large ( $\text{ACC}_{\text{SI}}$  is much higher compared to the amino acid free experiments), but at pH 10, this  
16 inhibitory effect is counteracted by the basic solution conditions such that the presence of high  
17 concentrations of both Gly and Asp do not result in a greatly increased  $\text{ACC}_{\text{SI}}$  compared to the amino  
18 acid-free experiments. The divergent response of ACC precipitation to the presence of amino acids at  
19 different seawater pH echoes the pH-dependent structural variations in ACC discussed with respect to  
20 the FTIR spectra above (Fig. 4), highlighting the importance of considering solution carbonate  
21 chemistry in concert with the Mg/Ca ratio and presence of additives.  
22  
23  
24  
25  
26  
27  
28  
29  
30

### 31 ***3.3 Relevance to marine calcifiers***

32  
33 We were unable to precipitate ACC within the pH and DIC range thought to characterise tropical  
34 zooxanthellate corals<sup>26,35,36</sup> in seawater with a Mg/Ca ratio close to natural (53/10.3 mM; Fig. 2), and  
35 the addition of amino acids serves to inhibit ACC precipitation (Fig. 8E). However, raising the  
36 seawater  $[\text{Ca}^{2+}]$  or lowering  $[\text{Mg}^{2+}]$  can reduce the DIC and  $[\text{CO}_3^{2-}]$  necessary to precipitate ACC (Fig.  
37 8). As such, we consider whether ACC can be produced within the DIC and pH range of marine  
38 calcifiers through a modification of the Mg/Ca ratio of the calcifying space. Fig. 10 summarises the  
39 effects of these processes in a quantitative manner, displaying the  $[\text{CO}_3^{2-}]$  necessary for ACC to  
40 precipitate from seawater as a function of both seawater  $[\text{Mg}^{2+}]$  and  $[\text{Ca}^{2+}]$ . This exercise highlights  
41 two important aspects of our dataset. Firstly, raising the initial seawater  $[\text{Ca}^{2+}]$  from 10.3 to 15-50  
42 mM results in a greatly reduced  $[\text{CO}_3^{2-}]$  required for ACC precipitation, whilst the degree to which  
43 this is the case is sensitive to seawater pH. At a lower, more biologically-relevant pH of 9.5, ACC  
44 precipitation occurs at a  $[\text{CO}_3^{2-}] \sim 2.5$  mM lower compared to pH 10 (possibly because it differs  
45 structurally), such that the necessary  $[\text{CO}_3^{2-}]$  to form ACC can be reduced to well within the range of  
46 that reconstructed for marine calcifiers. Secondly, whilst lowering the seawater  $[\text{Mg}^{2+}]$  can also result  
47 in a reduction in the  $[\text{CO}_3^{2-}]$  required to precipitate ACC, the extent to which this is the case is even  
48 more strongly dependent on the solution carbonate chemistry, and reducing  $[\text{Mg}^{2+}]$  is a less efficient  
49 mechanism by which the necessary  $[\text{CO}_3^{2-}]$  for ACC precipitation can be reduced (Fig. 10). Moreover,  
50 there is a limit to the extent to which the  $[\text{CO}_3^{2-}]$  required to induce ACC precipitation can be reduced  
51  
52  
53  
54  
55  
56  
57  
58  
59  
60

1  
2  
3 by lowering  $[\text{Mg}^{2+}]$ . The experiments in seawater with 10 mM  $\text{Mg}^{2+}$  and DIC at the lower end of the  
4 range investigated likely represent ACC-calcite mixtures (Fig. 7D), and further decreasing the initial  
5 seawater Mg/Ca ratio resulted in calcite precipitation.  
6  
7

8 In summary, these results indicate that manipulation of the calcification site Mg/Ca ratio may enable  
9 ACC to be precipitated at a relatively low DIC. However, applying this finding to the tropical  
10 zooxanthellate corals results in a discrepancy. Although the presence of an ACC precursor phase has  
11 been reported for these organisms,<sup>10,56</sup> several studies using independent techniques have shown that  
12 the  $[\text{Ca}^{2+}]$  at the calcification site of corals is unlikely to be elevated above  $\sim 15$  mM.<sup>26,43,57</sup> ACC  
13 precipitation at this  $[\text{Ca}^{2+}]$  required a  $[\text{CO}_3^{2-}]$  of  $>8$  mM in our experiments (Fig. 10), far exceeding  
14 that thought to occur at the biomineralization site of these corals.<sup>26,28,43,57,58</sup> We also note that the  
15 experimental transformation of inorganic ACC to aragonite is a long process, taking  $\sim 10$  days in  
16 seawater with the normal Mg/Ca ratio and proceeding through an intermediate monohydrocalcite  
17 phase.<sup>19</sup> Lastly, it may be difficult to reconcile observed skeletal trace element distribution  
18 coefficients with a greatly elevated  $[\text{Ca}^{2+}]$ .<sup>24</sup> It is beyond the scope of this study to address this issue  
19 directly, except to highlight that reconciliation of our precipitation data with that from corals either  
20 requires the role of ACC in corals to be reconsidered, or for a mechanism to be found by which the  
21 DIC necessary to precipitate ACC can be reduced without greatly modifying the seawater Mg/Ca  
22 ratio. Irrespective, one specific area in which our results can directly inform the ongoing debate  
23 regarding ACC as a possible precursor to coral aragonite (cf. refs. 59,60) concerns the interpretation  
24 of Raman spectra. A distinguishing feature of ACC is the greatly increased  $\nu_1$  FWHM relative to  
25 crystalline  $\text{CaCO}_3$  and lack of visible lattice mode vibrations (Fig. 7). Pertinently, we show that  
26 material precipitated under certain conditions has spectral features of both ACC and calcite (Fig. 3E),  
27 and likely represents ACC-calcite mixtures (Fig. 7D). Care should be taken in the identification of  
28 biological ACC based on Raman spectra that contain lattice mode vibrations. Whilst lattice mode  
29 vibrations do not necessarily rule out the presence of an amorphous phase, the presence or position of  
30 lattice mode vibrations alone are not indicative of ACC.  
31  
32  
33  
34  
35  
36  
37  
38  
39  
40  
41  
42  
43  
44  
45

46 In contrast to marine calcifiers that build an aragonitic skeleton, our data are not necessarily difficult  
47 to reconcile with biomineralization in organisms that produce a low-Mg calcite shell such as the  
48 planktonic foraminifera. These organisms have also been suggested to calcify through an ACC  
49 precursor,<sup>11,12</sup> but crucially there is consensus that the Mg/Ca ratio at the site of calcification must be  
50 greatly reduced below that of seawater in order to promote the formation of low-Mg calcite.<sup>13,30,61</sup>  
51 However, at present little is known about the calcification site DIC in foraminifera. A more detailed  
52 comparison to our inorganic ACC precipitation data will require better constraint of this aspect of  
53 foraminifera calcification.  
54  
55  
56  
57  
58  
59  
60

#### 4. Conclusion



1  
2  
3 The control that pH and DIC, the concentration of  $[Mg^{2+}]$  and  $[Ca^{2+}]$ , and the presence of different  
4 concentrations of Asp, Glu and Gly exert on the saturation state required to precipitate ACC from  
5 seawater ( $ACC_{SI}$ ) was investigated. In normal seawater ( $Mg/Ca = 5$ ), the solution pH and DIC exert at  
6 most a minor control on  $ACC_{SI}$  and no resolvable structural control as evidenced by FTIR, Raman,  
7 XRD, and TGA-MS. The presence of high concentrations ( $>2$  mM) of amino acids inhibit ACC  
8 precipitation, but also do not alter the spectroscopic features or water of crystallisation of the  
9 precipitate. In contrast, lowering the seawater  $Mg/Ca$  ratio, either by reducing  $[Mg^{2+}]$  or increasing  
10  $[Ca^{2+}]$ , may greatly reduce the DIC and  $[CO_3^{2-}]$  necessary to precipitate, yet can result in a greater  
11 degree of short and long-range order, as evidenced by the appearance of lattice-mode vibrations, a  
12 narrower  $\nu_3$  Raman peak, and a greatly reduced water of crystallisation.  
13  
14  
15  
16  
17  
18  
19

20  
21 In addition, we investigate the combined effect of varying the seawater carbonate chemistry and  
22  $[Mg^{2+}]$ ,  $[Ca^{2+}]$  or amino acid concentration on the structure of ACC and  $ACC_{SI}$ . Whilst we find no  
23 substantial direct impact of pH or DIC on ACC structure precipitated from unmodified seawater (see  
24 above), these experiments highlight the differing impact of the seawater  $Mg/Ca$  ratio and  
25 concentration of amino acids at lower pH. In general, modifying  $Mg/Ca_{sw}$  exerts a much greater  
26 control on both the structure of ACC and  $ACC_{SI}$  at pH 9-9.6 compared to pH 10, the latter typical of  
27 much inorganic ACC work, highlighting the need to consider the solution carbonate chemistry in  
28 tandem with other variables.  
29  
30  
31  
32  
33

34  
35 Finally, we find that the DIC required to precipitate ACC from normal seawater greatly exceeds that  
36 thought to characterise the calcifying space of certain marine organisms that may utilise this pathway.  
37 The only variable investigated here which resulted in a large, systematic decrease in the DIC required  
38 to precipitate ACC is the seawater  $Mg/Ca$  ratio, raising the possibility that modifying the seawater  
39  $Mg/Ca$  ratio through Mg removal or Ca addition is an important component of utilising an ACC  
40 pathway.  
41  
42  
43  
44  
45

46 **Supporting Information.** Further methodological details, additional TGA-MS results, and an in-  
47 depth assessment of the multiple linear regression models relating  $ACC_{SI}$  to the experimental  
48 variables. Supplementary Tab. 1 presents full seawater chemistry details for all precipitates.  
49  
50

## 51 **Acknowledgement**

52 This work was supported by the Leverhulme Trust (Research project grant 2015-268 to NA, RK, and  
53 KP). The Royal Society is gratefully acknowledged for the award of an Industry Fellowship to P.B.W.  
54 We are thankful to Laetitia Pichevin for assistance in analysing seawater samples by ICP-OES.  
55  
56  
57  
58  
59  
60

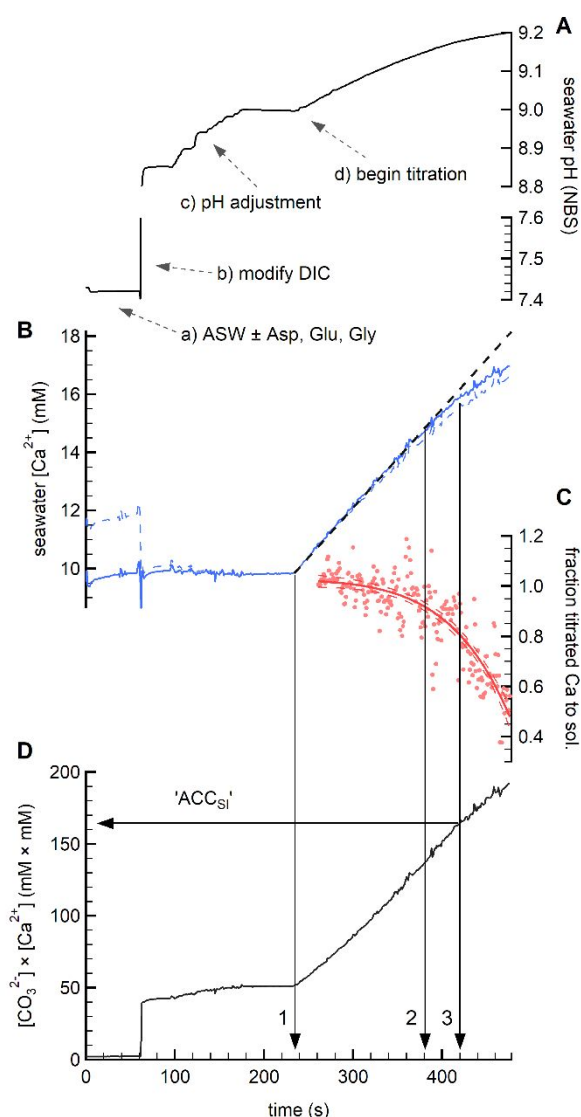


**Figure 1:** An example titration curve to induce ACC precipitation from seawater. (A) pH evolution over the course of the titration, note break in y-axis scale. In this case, (i) artificial seawater is (ii) spiked with 1 M  $Na_2CO_3$  to achieve the desired DIC for the experiment. (iii) The pH is then adjusted using HCl or NaOH, and the solution is equilibrated for 60 s. (iv) ACC precipitation is induced by simultaneous titration of 0.45 M  $Na_2CO_3$  and  $CaCl_2$ . A pH increase occurs as ACC precipitation is not immediate. (B) Seawater  $[Ca^{2+}]$  measured in real-time using a calibrated ISE. Dashed and solid blue lines show the measurement both uncorrected and corrected for pH change, as pH exerts a minor control on the measured electrode voltage. The dashed black line shows the predicted evolution of seawater  $Ca^{2+}$  if no precipitation takes place. The divergence of the Ca electrode measurement from this line therefore indicates the onset of precipitation. (C) The fraction Ca titrated that went into solution, based on the divergence of the curves shown in panel B. Vertical arrows (1) show the onset of titration, (2) the divergence of the measured solution  $Ca^{2+}$  from predicted, indicating the initiation of precipitation, and (3) the point at which more than 20% of the titrated Ca was utilised in ACC precipitation. (D) The temporal evolution of the product of  $[Ca^{2+}]$  and  $[CO_3^{2-}]$ , the latter calculated from DIC and pH using co2sys.<sup>36</sup> In the text and subsequent figures the seawater saturation state required to precipitate ACC (abbreviated 'ACC<sub>SI</sub>') is calculated as being the  $[Ca^{2+}][CO_3^{2-}]$  product at the location of arrow 3.

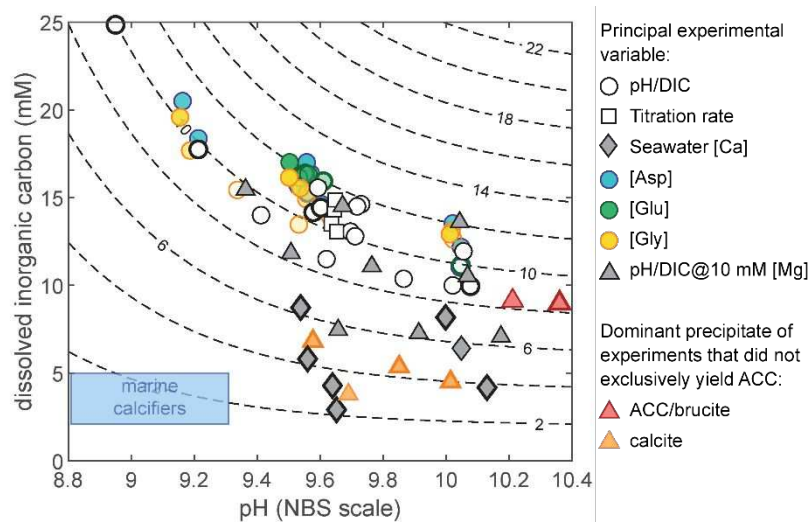


**Figure 2:** The pH and DIC range over which ACC was precipitated from seawater in this study. DIC and pH broadly co-varied in our experiments as it was not possible to precipitate ACC from (e.g.) low-pH, low-DIC seawater without modifying the seawater Mg/Ca ratio. The approximate upper range of estimates of carbonate chemistry at the site of biomineralisation in tropical zooxanthellate corals and foraminifera is shown for comparison (transparent blue box, note that the calcification site DIC estimates relate only to corals).<sup>27,28,36</sup> Contours show lines of equal  $[\text{CO}_3^{2-}]$  in mM. In most cases ACC was precipitated from solutions with a  $[\text{CO}_3^{2-}]$  of  $10 \pm 2$  mM, approximately equivalent to a seawater  $\text{Ca}^{2+}/\text{CO}_3^{2-}$  ratio of 1. Amino acid concentration is shown as a function of opacity, lighter symbols indicate lower concentrations. Bold symbols indicate experiments for which solution chemistry was directly measured, others are calculated following the method outlined in Fig. 1.

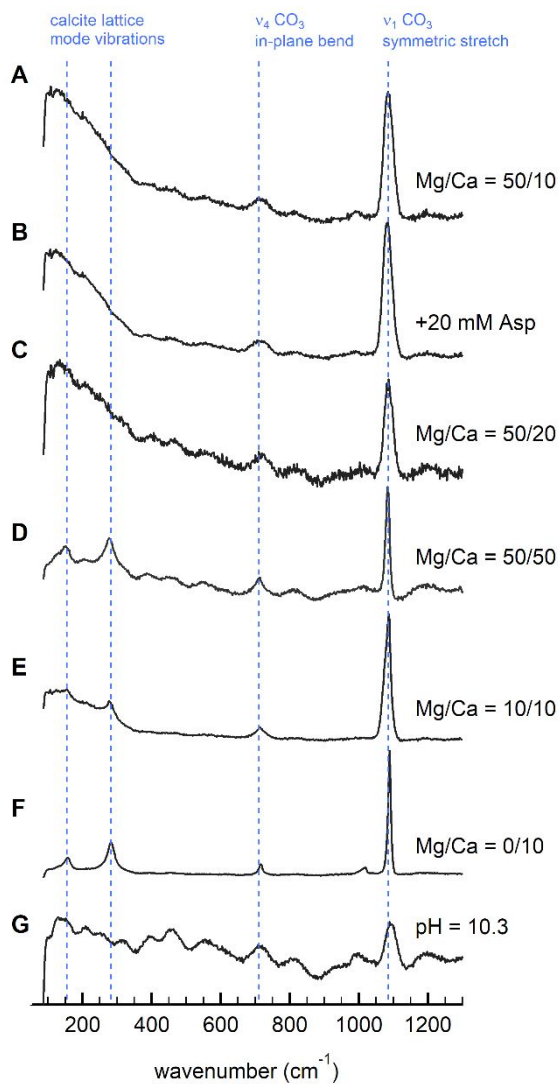


**Figure 3.** Representative Raman spectra of the inorganic precipitates. No processing was applied except for a linear baseline correction. Mg/Ca labels give the concentration of both elements in mM. All spectra show the characteristic features of ACC, except for F (calcite), and G, precipitated under extreme basic conditions (pH 10.3). At low Mg/Ca<sub>sw</sub> ratios the lattice mode vibrations of calcite become visible (D, E).

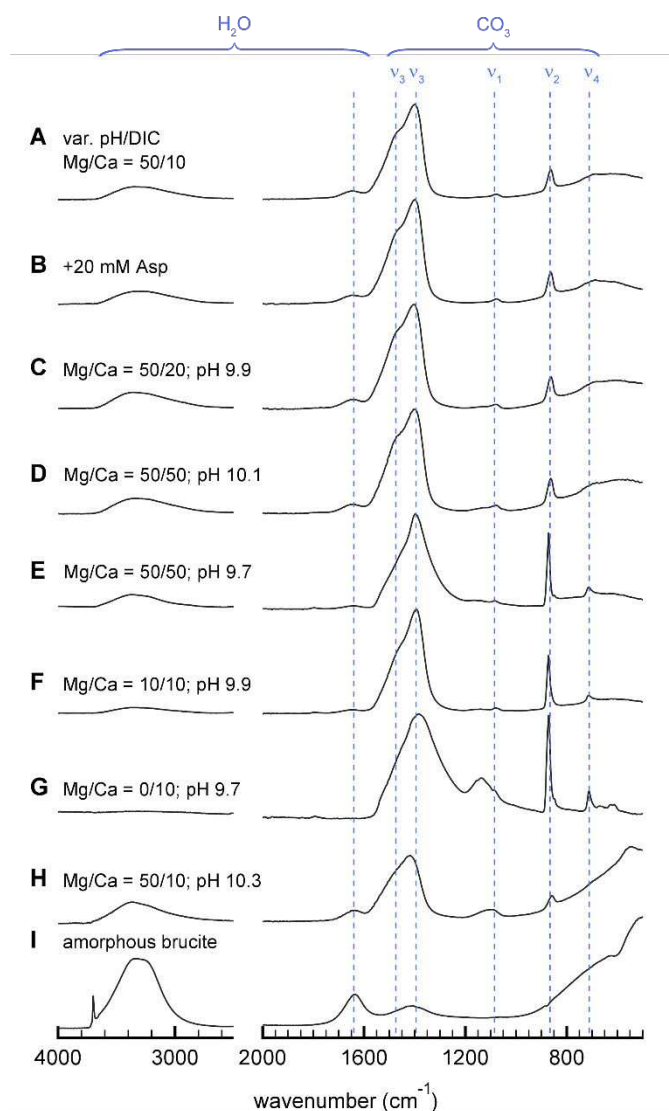


**Figure 4:** Representative baseline-corrected ATR-FTIR spectra of the precipitates. Mg/Ca labels give the concentration of both elements in mM. Spectra A-F are of ACCs, which have a characteristic split  $\nu_3$  vibration at 1410 and 1474  $\text{cm}^{-1}$ , G is calcite, and H, precipitated under extreme basic conditions, is an ACC-amorphous brucite mixture. Amorphous hydrated brucite is shown for comparison in I, prepared by pipetting 1 M  $\text{MgCl}_2$  into deionised water at pH 11, achieved through NaOH addition. Note the structural differences between D, E and F, precipitated under the same seawater Mg/Ca ratio, but at different pH and absolute  $[\text{Mg}^{2+}]$  and  $[\text{Ca}^{2+}]$ . The peak at 1648  $\text{cm}^{-1}$  is an OH vibration,<sup>16</sup> and does not indicate a brucite component in the ACC samples.

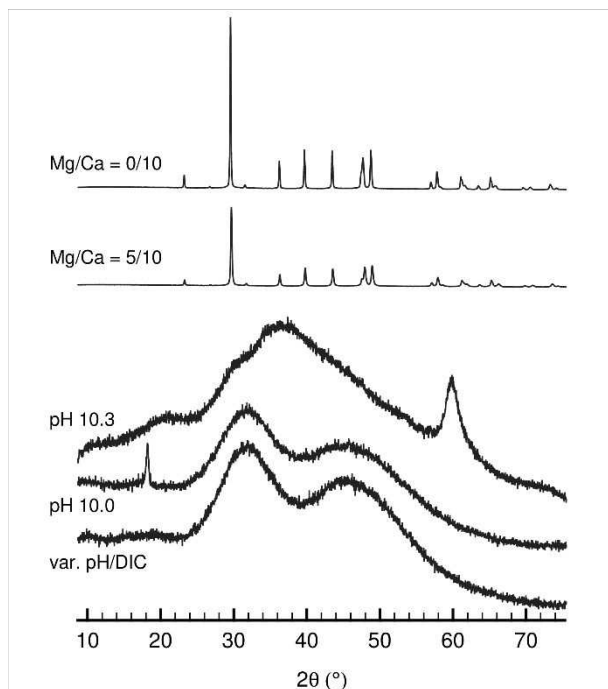


**Figure 5:** Representative XRD spectra of selected precipitates. A characteristic spectrum from the variable pH/DIC experiment is shown at the bottom of the figure. The broadly featureless spectrum confirms the amorphous or nanocrystalline nature of these samples. The only deviations from this spectrum were those of precipitates formed at high pH, which contain small, unidentifiable peaks, and at low seawater  $[\text{Mg}^{2+}]$  ( $<10$  mM), which are partly or entirely calcite.

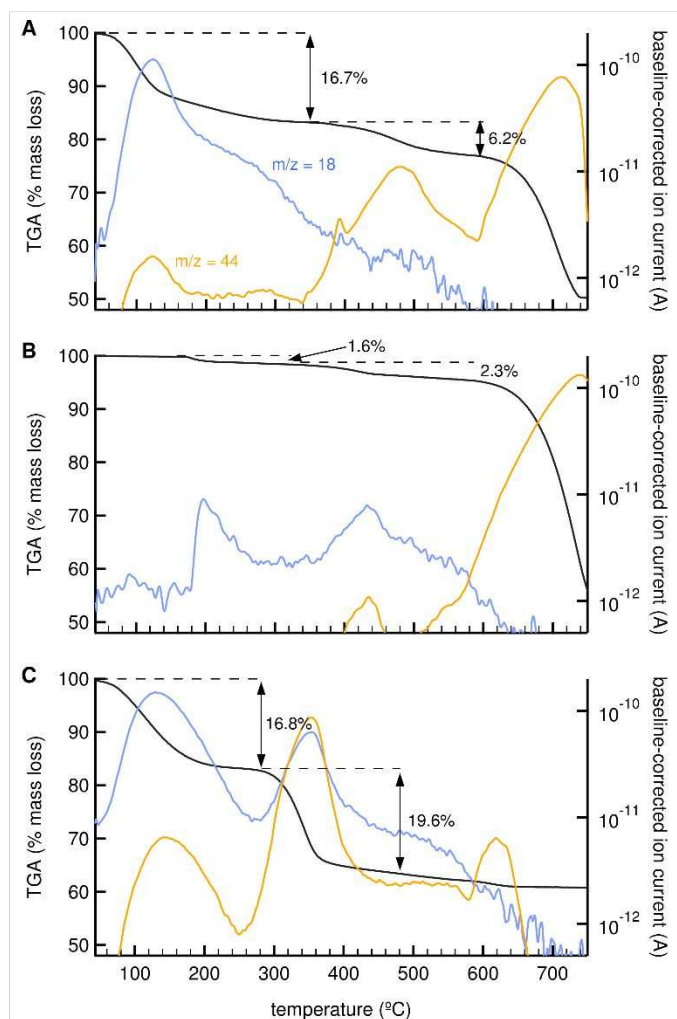


**Figure 6:** TGA-MS profiles of three endmember precipitates. Products of decomposition are shown in blue ( $\text{H}_2\text{O}$ ,  $m/z = 18$ ) and yellow ( $\text{CO}_2$ ,  $m/z = 44$ ). (A) ACC precipitated in seawater at pH 8.95 with a Mg/Ca ratio close to natural ( $\sim 5 \text{ mol mol}^{-1}$ ), showing the characteristic three-stage decomposition of these inorganic ACCs. (B) Calcite precipitation from seawater, achieved by reducing the seawater  $[\text{Mg}^{2+}]$  by a factor of 10 compared to natural (5 mM). (C) Amorphous material precipitated at the basic extreme of the pH range investigated (10.3 on the NBS scale). The FTIR spectra of this material indicates that it is an amorphous  $\text{CaCO}_3$ -brucite mixture.

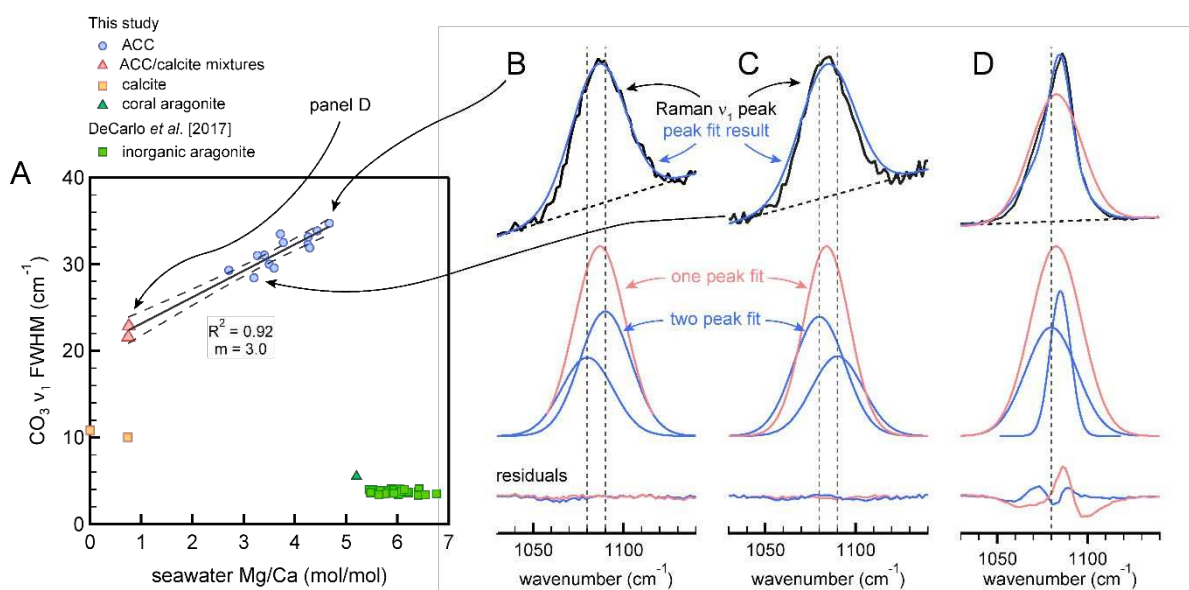


**Figure 7:** (A) Solution chemistry control on the Raman  $\nu_1$  ( $\text{CO}_3$  symmetric stretch) FWHM at  $\sim 1080$   $\text{cm}^{-1}$  of ACCs precipitated from seawater, compared to calcite precipitated under similar carbonate chemistry conditions (see the Supplementary Information), inorganic aragonite,<sup>43</sup> and a natural coral aragonite (*Porites* spp.). The latter is plotted assuming that corals precipitate aragonite from seawater with an unmodified Mg/Ca ratio, which may not be the case.<sup>26</sup> (B-D) Gaussian peak fitting of the  $\nu_1$  band of three selected amorphous precipitates spanning the investigated range of seawater Mg/Ca ratios. Panels B and C represent samples precipitated under different  $[\text{Ca}^{2+}_{\text{sw}}]$ , whereas D was precipitated with  $\text{Mg}^{2+}_{\text{sw}}$  reduced from 53 to 10 mM. The  $\nu_1$  band in ACCs precipitated under variable  $[\text{Ca}^{2+}_{\text{sw}}]$  is symmetric (these spectra can be fit equally well with one or two peaks). In contrast, ACC precipitated at the lowest seawater Mg/Ca ratio is characterised by an asymmetric  $\nu_1$  band which is best modelled by two peaks with different widths. This suggests that these precipitates are physical mixtures of low-Mg ACC and calcite.



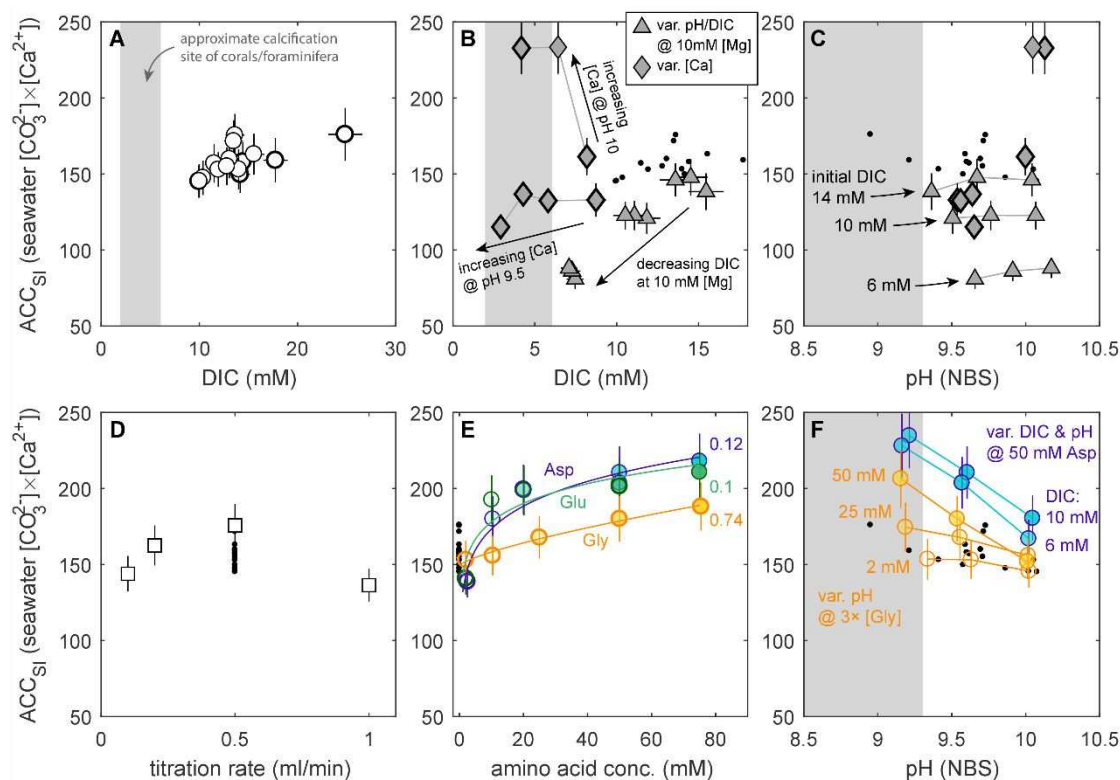


**Figure 8:** The control exerted by solution carbonate chemistry, Mg/Ca ratio and amino acid concentration on  $ACC_{SI}$ , the seawater saturation state necessary to precipitate ACC. Bold symbols are experiments for which solution chemistry was directly measured, others are calculated following the method outlined in Fig. 1. Vertical grey bars delineate the approximate range of DIC and pH at the site of biomineralisation in tropical zooxanthellate corals and foraminifera.<sup>21,25</sup> (A)  $ACC_{SI}$  as a function of DIC. Only the amino acid-free experiments in normal seawater (Mg/Ca = ~5) are shown. (B) The differential response of  $ACC_{SI}$  to reducing Mg/Ca<sub>sw</sub> through varying seawater [Mg<sup>2+</sup>] and [Ca<sup>2+</sup>]. Both adjustments result in ACC precipitation at lower DIC compared to the experiments in normal seawater (black dots from panel A). (C) The effect of varying pH and DIC in seawater with a reduced Mg/Ca ratio (10 mM Mg<sup>2+</sup> instead of 53 mM or 20-50 mM Ca<sup>2+</sup> instead of 10 mM, see panel B for legend). Lines join experiments of equivalent initial DIC at different pH. Note that the low DIC experiments may contain a calcite component (Fig. 7D). (D) Titration rate exerts no systematic effect on  $ACC_{SI}$ . (E) The impact of amino acid concentration on ACC precipitation. Power coefficients of least-squares regressions are shown. (F) The combined influence of varying pH/DIC in the presence of Asp and Gly. Low AA concentrations (2 mM) produce data that fall within the range of the additive-free experiments (black dots from panel A), higher concentrations strongly inhibit ACC precipitation at lower, more biologically relevant pH, but to a much lesser extent at high pH. Amino acid concentration is shown as a function of symbol opacity in panels E and F.

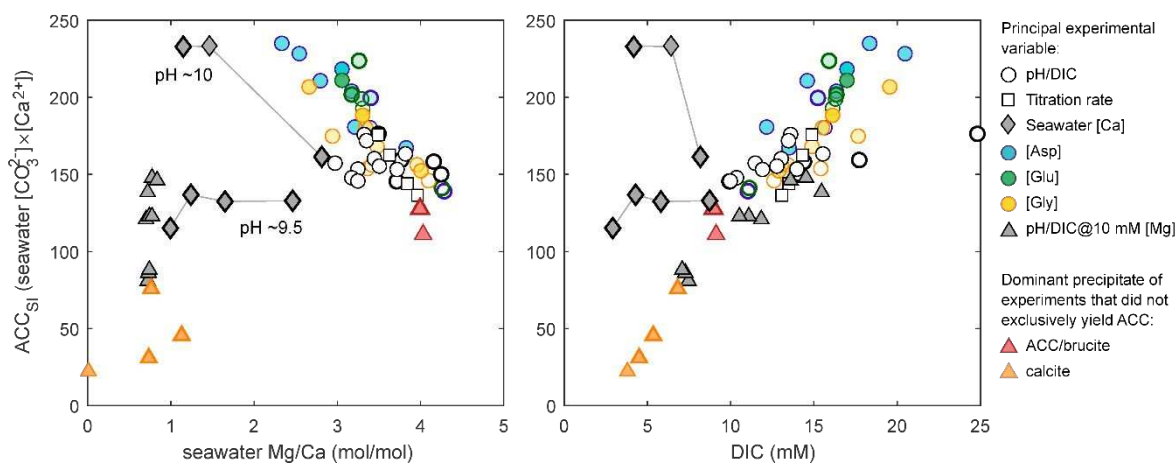


**Figure 9:** Combining the data shown in Fig. 8 to examine the overall controls of solution chemistry on  $ACC_{SI}$ , the seawater saturation state required to induce ACC precipitation. Most experiments, especially those performed in the presence of amino acids, fall on a negative  $ACC_{SI}$ -Mg/ $Ca_{sw}$  array and positive  $ACC_{SI}$ -DIC array, indicating that the inhibitive effect of these additives is overcome through  $Ca^{2+}$  and/or DIC titration (see also the multiple linear regression models in Tab. 2). Error bars are omitted for clarity (see Fig. 8).

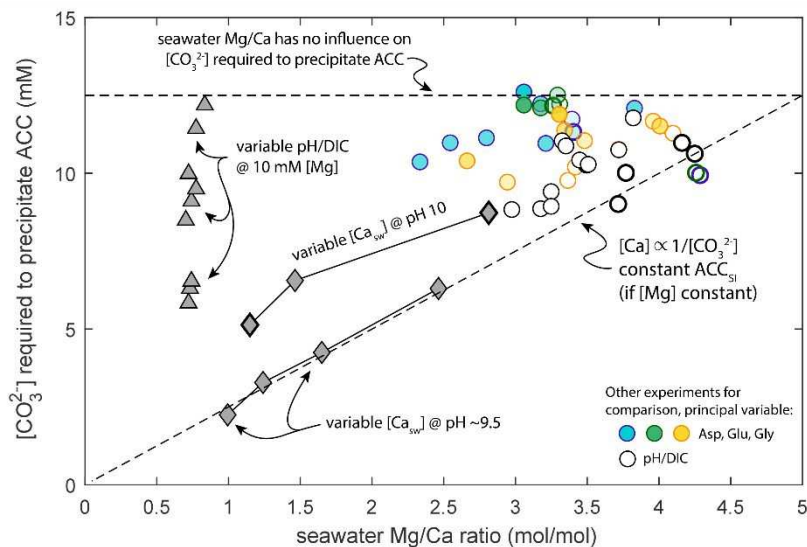


**Figure 10:** Comparing strategies to reduce the  $[\text{CO}_3^{2-}]$  necessary for ACC precipitation from seawater;  $\text{Mg}^{2+}$  removal (triangles) or  $\text{Ca}^{2+}$  addition (diamonds). Data from experiments in which  $\text{Mg}/\text{Ca}_{\text{sw}}$  was not the principal variable are shown for comparison (circles). Dashed lines show hypothetical endmember scenarios of the relationship between ACC precipitation and solution chemistry. Almost no data lie on the horizontal dashed line, with the exception of experiments that contained high concentrations of amino acids, demonstrating that reducing  $\text{Mg}/\text{Ca}_{\text{sw}}$  either by raising the seawater  $[\text{Ca}^{2+}]$  or reducing  $[\text{Mg}^{2+}]$  lowers the  $[\text{CO}_3^{2-}]$  necessary for ACC precipitation. In addition, these data highlight the interplay of solution elemental and carbonate chemistry. At a higher (less biologically relevant) pH, raising  $[\text{Ca}^{2+}_{\text{sw}}]$  results in a reduction in the required  $[\text{CO}_3^{2-}]$  required to precipitate ACC, but to a lesser extent than at pH 9.5, demonstrating that ACC precipitation is differently (more) sensitive to  $[\text{Ca}^{2+}_{\text{sw}}]$  at lower pH.

**Table 1:** Overview of the investigated factors impacting ACC precipitation from seawater. The carbonate chemistry details represent those at the onset of precipitation (i.e. at ACC<sub>SI</sub>), whereas the seawater [Mg<sup>2+</sup>] and [Ca<sup>2+</sup>] are those at the start of the experiment. See the Supplementary Information for full details.

Principal experimental variable	n	DIC (mM) at ACC <sub>SI</sub>	pH (NBS) at ACC <sub>SI</sub>	Titration rate (ml/min)	Amino acid conc. (mM)	Initial seawater [Mg] (mM)	Initial seawater [Ca] (mM)	Detailed sample ID (see SI)
pH & DIC	14	10.0-24.9	9.0-10.1	0.5	-	53	10.3	1-1, 1-2, 1-3, 1-13
Titration rate	4	13.0-14.9	9.6	0.1-1.0	-	53	10.3	1-15, 1-16
pH & DIC in low-Mg (10 mM) seawater	3×3	7.1-15.5	9.4-10.2	0.5	-	10	10.3	1-17
[Ca] @ 2×pH	3	3.0-8.7	9.5-9.7	0.5	-	53	15.0-45.0	1-6, 1-7
	4	4.2-8.2	10.0-10.1				20.0-50.0	2-19
pH & DIC with 50 mM Asp	6	12.2-20.5	9.2-10.0	0.5	50	53	10.3	-
[Asp]	5	11.0-17.0	9.5-10.0	0.5	2.5-75	53	10.3	1-4, 1-10
[Glu]	5	11.1-17.0	9.5-10.0	0.5	2-75	53	10.3	1-5, 1-11
[Gly] @ 3×pH	11	12.6-19.6	9.2-10.0	0.5	2-75	53	10.3	-
[Mg] & [Ca] @ Constant Mg/Ca	2	3.0,14.5	9.7	0.5	-	53,10	50,10.3	-
Mg-free SW	1	3.8	9.7	0.5	-	0.1	10.3	1-8
High pH extreme	2	9.0-9.1	10.2-10.4	0.5	-	53	10.3	1-9

**Table 2:** Gradients and goodness of fit of multiple linear regression models through subsets of the ACC precipitation data shown in Fig. 2 and summarised in Tab. 1. The models were produced twice, both with and without amino acid concentration as an independent variable, otherwise taking the form defined in Eq. 2 (see text for rationale). The variable pH/DIC model was also performed twice, both with and without one outlier removed (the highest DIC data point in Fig. 8A, based on its Cook's distance). Coefficient uncertainties are 1SE except where noted. Bold values denote independent variables that are significant predictors of ACC<sub>SI</sub> at the 95% CI. Note that a coefficient p value >0.05 does not necessarily imply that the predictor is not significant, as this can also arise from covariance in the predictors (e.g. amino acid concentration and Mg/Ca<sub>sw</sub>; Fig. 9). The units of the slopes for Mg/Ca<sub>sw</sub>, pH, DIC, and [AA] are mol/mol<sup>-1</sup>, unit<sup>-1</sup>, mM<sup>-1</sup>, and mM<sup>-1</sup> respectively.

Principal variable:	pH/DIC		pH/DIC Exc. one outlier		Aspartic acid conc.		Glutamic acid conc.‡		Glycine conc.		pH/DIC in low-Mg (10 mM) seawater		Entire dataset†	
	m*	p*	m*	P*	m	p	m	p	m	p	m	p	m	p
Amino acid concentration used in multiple linear regression model														
Mg/Ca <sub>sw</sub>	-9.4±5.6	0.15	<b>-16.2±4.0</b>	0.01	-10.4±9.6	0.33	-9.1		-40.0±23.6	0.14	16.5±106.1	0.882	<b>-30.0±4.6</b>	4.3×10 <sup>-7</sup>
pH	24.3±16.6	0.14	<b>37.6±11.8</b>	0.01	<b>-96.1±35.5</b>	0.04	74.4		40.7±25.6	0.16	25.3±16.9	0.195	<b>47.5±14.2</b>	2.0×10 <sup>-3</sup>
DIC	<b>4.0±1.2</b>	0.01	<b>7.1±1.4</b>	5×10 <sup>-4</sup>	-4.9±3.3	0.19	16.2		4.0±2.7	0.19	<b>8.8±1.3</b>	9.1×10 <sup>-4</sup>	<b>8.7±1.6</b>	3.5×10 <sup>-6</sup>
[AA]	-	-	-	-	<b>0.6±0.2</b>	0.02	0.1		0.2±0.1	0.06	-	-	0.17±0.09	0.06
<b>Overall model:</b>														
R <sup>2</sup>	0.66		0.79		0.98		1.00		0.95		0.98		0.89	
p	0.01		2.0×10 <sup>-3</sup>		1.9×10 <sup>-4</sup>				4.5×10 <sup>-4</sup>		1.8×10 <sup>-4</sup>		1.3×10 <sup>-15</sup>	
RMSE	6.9		5.2		5.6				5.4		5.1		9.3	
Amino acid concentration <b>not</b> used in multiple linear regression model														
Mg/Ca <sub>sw</sub>	As above		As above		<b>-35.8±9.1</b>	7.5×10 <sup>-3</sup>	-30.9±9.5	0.19	<b>-62.8±27.3</b>	0.05	As above		<b>-33.5±4.2</b>	2.1×10 <sup>-9</sup>
pH					1.6±30.5	0.96	101.2±21.1	0.13	<b>77.5±25.6</b>	0.02			<b>64.0±11.7</b>	4.0×10 <sup>-6</sup>
DIC					3.5±3.3	0.34	14.9±3.3	0.82	5.3±3.4	0.16			<b>10.7±1.2</b>	2.6×10 <sup>-10</sup>
<b>Overall model:</b>														
R <sup>2</sup>					0.94		1.00		0.91				0.88	
p					4.9×10 <sup>-4</sup>		0.02		5.4×10 <sup>-4</sup>				7.6×10 <sup>-16</sup>	
RMSE					9.0		0.8		6.8				9.7	

\*These estimates represent the median±2SD values of a Monte Carlo simulation (1000 models) including normally-distributed uncertainty in both dependent and independent variables. For all other models the least-squares regression through the best estimate of all data are shown. See the SI for a demonstration that there is no significant difference between the two approaches.

‡There are insufficient data from this subset of experiments to reliably estimate coefficient or model uncertainties for this number of independent variables.

†The experiments conducted in low-Mg seawater were excluded from this regression model as some precipitates are likely ACC-calcite mixtures (see text). The model that uses amino acid concentration as a predictor considers all amino acids together, i.e. Asp, Glu, and Gly were not included as separate terms. This choice makes little difference to the result (see the SI).

## References

- (1) Hodson, M. E.; Benning, L. G.; Demarchi, B.; Penkman, K. E. H.; Rodriguez-Blanco, J. D.; Schofield, P. F.; Versteegh, E. A. A. Biomineralisation by earthworms – an investigation into the stability and distribution of amorphous calcium carbonate *Geochem. Trans.* **2015**, *16* (4), doi:10.1186/s12932-015-0019-z.
- (2) Addadi, L.; Raz, S.; Weiner, S. Taking advantage of disorder: Amorphous calcium carbonate and its roles in biomineralization *Adv. Mater.* **2003**, *15*, 959–970.
- (3) Taylor, M. G.; Simkiss, K.; Greaves, G. N.; Okazaki, M.; Mann, S. An X-ray absorption spectroscopy study of the structure and transformation of amorphous calcium carbonate from plant cystoliths *Proc. R. Soc. B Biol. Sci.* **1993**, *252*, 75–80.
- (4) Weiner, S.; Levi-Kalishman, Y.; Raz, S.; Addadi, L. Biologically formed amorphous calcium carbonate *Connect. Tissue Res.* **2003**, *44*, 214–218.
- (5) Aizenberg, B. J.; Lambert, G.; Addadi, L.; Weiner, S. Stabilization of amorphous calcium carbonate by specialized macromolecules in biological and synthetic precipitates *Adv. Mater.* **1996**, *8*, 222–226.
- (6) Beniash, E.; Aizenberg, J.; Addadi, L.; Weiner, S. Amorphous calcium carbonate transforms into calcite during sea urchin larval spicule growth Amorphous calcium carbonate transforms into calcite during sea urchin larval spicule growth *Proc. R. Soc. B Biol. Sci.* **1997**, *264*, 461–465.
- (7) Aizenberg, J.; Lambert, G.; Weiner, S.; Addadi, L. Factors Involved in the formation of amorphous and crystalline calcium carbonate : A study of an Ascidian skeleton *J. Am. Chem. Soc.* **2002**, *124*, 32–39.
- (8) Weiss, I. M.; Tuross, N.; Addadi, L.; Weiner, S. Mollusc larval shell formation: Amorphous calcium carbonate is a precursor phase for aragonite *J. Exp. Zool.* **2002**, *293*, 478–491.
- (9) Sviben, S.; Gal, A.; Hood, M. A.; Bertinetti, L.; Politi, Y.; Bennet, M.; Krishnamoorthy, P.; Schertel, A.; Wirth, R.; Sorrentino, A.; Pereiro, E.; Faivre, D.; Scheffel, A. A vacuole-like compartment concentrates a disordered calcium phase in a key coccolithophorid alga *Nat. Commun.* **2016**, *7*, doi:10.1038/ncomms11228.
- (10) Mass, T.; Giuffrè, A. J.; Sun, C.; Stiffler, C. A.; Frazier, M. J.; Neder, M.; Tamura, N.; Stan C. V.; Marcus, M. A.; Gilbert, P. U. P. A. *Proc. Natl. Acad. Sci.* **2017**, *114*, E7670-E7678.
- (11) Erez, J. The source of ions for biomineralization in foraminifera and their implications for paleoceanographic proxies *Rev. Miner. Geochem.* **2003**, *54*, 115-149.
- (12) Jacob, D. E.; Wirth, R.; Agbaje, O. B. A.; Branson, O.; Eggins, S. M. Planktic foraminifera form their shells via metastable carbonate phases *Nat. Commun.* **2017**, *8*, 1265.
- (13) Evans, D.; Müller, W.; Erez, J. Assessing foraminifera biomineralisation models through trace element data of cultures under variable seawater chemistry *Geochim. Cosmochim. Acta* **2018**, *236*, 198-217.
- (14) Schiebel, R. Planktic foraminiferal sedimentation and the marine calcite budget *Glob. Biogeochem. Cycles* **2002**, *16*, doi:10.1029/2001GB001459.
- (15) Henahan, M. J.; Evans, D.; Shankle, M.; Burke, J. E.; Foster, G. L.; Anagnostou, E.; Chalk, T. B.; Stewart, J. A.; Alt, C. H. S.; Durrant, J.; Hull, P. M. Size-dependent response of foraminiferal calcification to seawater carbonate chemistry *Biogeosciences* **2017**, *14*, 3287-3308.
- (16) Loste, E.; Wilson, R. M.; Seshadri, R.; Meldrum, F. C. The role of magnesium in stabilising amorphous calcium carbonate and controlling calcite morphologies *J. Cryst. Growth* **2003**, *254*, 206–218.
- (17) Bentov, S.; Weil, S.; Glazer, L.; Sagi, A.; Berman, A. Stabilization of amorphous calcium carbonate by phosphate rich organic matrix proteins and by single phosphoamino acids *J. Struct. Biology* **2010**, *171*, 207–215.
- (18) Stephens, C. J.; Ladden, S. F.; Meldrum, F. C.; Christenson, H. K. Amorphous calcium carbonate is stabilized in confinement *Adv. Funct. Mater.* **2010**, *20*, 2108–2115.
- (19) Zhang, Z.; Xie, Y.; Xu, X.; Pan, H.; Tang, R. Transformation of amorphous calcium carbonate into aragonite *J. Cryst. Growth* **2012**, *343*, 62–67.
- (20) Bots, P.; Benning, L. G.; Rodriguez-Blanco, J.-D.; Roncal-Herrero, T.; Shaw, S. Mechanistic insights into the crystallization of amorphous calcium carbonate (ACC) *Cryst. Growth Des.* **2012**, *12*, 3806–3814.
- (21) Lam, R. S. K.; Charnock, J. M.; Lennie, A.; Meldrum, F. C. Synthesis-dependant structural variations in amorphous calcium carbonate *Cryst. Eng. Comm.* **2007**, *9*, 1226–1236.
- (22) Levi-Kalishman, B. Y.; Raz, S.; Weiner, S.; Addadi, L.; Sagi, I. Structural differences between biogenic amorphous calcium carbonate phases using X-ray absorption spectroscopy *Adv. Funct. Mater.* **2002**, *12*, 43–48 (2002).
- (23) Bentov, S.; Brownlee, C.; Erez, J. The role of seawater endocytosis in the biomineralization process in calcareous foraminifera *Proc. Natl. Acad. Sci.* **2009**, *106*, 21500–21504.
- (24) Gagnon, A. C.; Adkins, J. F.; Erez, J. Seawater transport during coral biomineralization *Earth Planet. Sci. Lett.* **2012**, *329*, 150–161.
- (25) Tambutté, E.; Tambutté, S.; Segonds, N.; Zoccola, D.; Venn, A.; Erez, J.; Allemand, D. Calcein labelling and electrophysiology : insights on coral tissue permeability and calcification *Proc. R. Soc. B Biol. Sci.* **2012**, *279*, 19–27.
- (26) Al-horani, F. A.; Al-moghrabi, S. M.; de Beer, D. Microsensor study of photosynthesis and calcification

- 1  
2  
3 in the scleractinian coral , *Galaxea fascicularis* : active internal carbon cycle *J. Exp. Marine Biol. Ecol.* **2003**,  
4 288, 1–15.
- 5 (27) de Nooijer, L. J.; Toyofuku, T.; Kitazato, H. Foraminifera promote calcification by elevating their  
6 intracellular pH *Proc. Natl. Acad. Sci.* **2009**, *106*, 15374–15378.
- 7 (28) Allison, N.; Cohen, I.; Finch, A.; Erez, J.; Tudhope, A. W. Corals concentrate dissolved inorganic carbon  
8 to facilitate calcification *Nat. Commun.* **2014**, *5*, doi:10.1038/ncomms6741.
- 9 (29) Gaetani, G. A.; Cohen, A. L. Element partitioning during precipitation of aragonite from seawater : A  
10 framework for understanding paleoproxies *Geochim. Cosmochim. Acta* **2006**, *70*, 4617–4634.
- 11 (30) Bentov, S.; Erez, J. Impact of biomineralization processes on the Mg content of foraminiferal shells: A  
12 biological perspective *Geochemistry Geophys. Geosystems* **2006**, *7*, doi:10.1029/2005GC001015.
- 13 (31) Inoue, M.; Gussone, N.; Koga, Y.; Iwase, A.; Suzuki, A.; Sakai, K.; Kawahata, H. Controlling factors of  
14 Ca isotope fractionation in scleractinian corals evaluated by temperature, pH and light controlled culture  
15 experiments *Geochim. Cosmochim. Acta* **2015**, *167*, 80–92.
- 16 (32) Giuffrè, A. J.; Gagnon, A. C.; De Yoreo, J. J.; Dove, P. M. Isotopic tracer evidence for the amorphous  
17 calcium carbonate to calcite transformation by dissolution-reprecipitation *Geochim. Cosmochim. Acta* **2015**,  
18 *165*, 407–417.
- 19 (33) Faatz, B. M.; Gröhn, F.; Wegner, G. Amorphous calcium carbonate: Synthesis and potential intermediate  
20 in biomineralization *Adv. Funct. Mater.* **2004**, *16*, 996-1000.
- 21 (34) Ogino, T.; Suzuki, T.; Sawada, K. The formation and transformation mechanism of calcium carbonate in  
22 water *Geochim. Cosmochim. Acta* **1987**, *51*, 2757–2767.
- 23 (35) Cai, W. J.; Ma, Y.; Hopkinson, B. M.; Grottoli, A. G.; Warner, M. E.; Ding, Q.; Hu, X.; Yuan, X.;  
24 Schoepf, V.; Xu, H.; Han, C.; Melman, T. F.; Hoadley, K. D.; Pettay, D. T.; Matsui, Y.; Baumann, J. H.; Levas,  
25 S.; Ying, Y.; Wang, Y. Microelectrode characterization of coral daytime interior pH and carbonate chemistry  
26 *Nat. Commun* **2016**, *7*, doi:10.1038/ncomms11144.
- 27 (36) McCulloch, M. T.; D’Olivo Cordero, J. P.; Falter, J.; Holcomb, M.; Trotter, J. A. Coral calcification in a  
28 changing World and the interactive dynamics of pH and DIC upregulation *Nat. Commun.* **2017**, *8*,  
29 doi:10.1038/ncomms15686.
- 30 (37) Wang, D.; Wallace, A. F.; De Yoreo, J. J.; Dove, P. M. Carboxylated molecules regulate magnesium  
31 content of amorphous calcium carbonates during calcification *Proc. Natl. Acad. Sci.* **2009**, *106*, 21511–21516.
- 32 (38) Whittaker, M. L.; Sun, W.; DeRocher, K. A.; Jayaraman, S.; Ceder, G.; Joester, D. Structural basis for  
33 metastability in amorphous calcium barium carbonate (ACBC) *Adv. Funct. Mater.* **2017**, *28*, 1704202.
- 34 (39) Millero, F. J. *Chemical Oceanography* (4<sup>th</sup> Ed.) CRC Press: Boca Raton, FL, **2013**.
- 35 (40) Lewis E.; Wallace D. CO2SYS-Program developed for the CO<sub>2</sub> system calculations. ORNL/CDIAC-105.  
36 Carbon Dioxide Information Analysis Center, Oak Ridge National Laboratory, US Department of Energy, Oak  
37 Ridge, Tennessee, US, **2006**.
- 38 (41) Blue, C. R.; Giuffrè, A.; Mergelsberg, S.; Han, N.; De Yoreo, J. J.; Dove, P. M. Chemical controls on the  
39 magnesium content of amorphous calcium carbonate *Geochim. Cosmochim. Acta* **2017**, *196*, 179–196.
- 40 (42) Wang, D.; Hamm, L. M.; Bodnar, R. J.; Dove, P. M. Raman spectroscopic characterization of the  
41 magnesium content in amorphous calcium carbonates *J. Raman Spectrosc.* **2012**, *43*, 543–548.
- 42 (43) DeCarlo, T. M.; D’Olivo, J. P.; Foster, T.; Holcomb, M.; Becker, T.; McCulloch, M. T. Coral calcifying  
43 fluid aragonite saturation states derived from Raman spectroscopy *Biogeosciences*, **2017**, *14*, 5253–5269.
- 44 (44) Tobler, D. J.; Blanco, J. D. R.; Dideriksen, K.; Sand, K. K.; Bovet, N. The effect of aspartic acid and  
45 glycine on amorphous calcium carbonate (ACC) structure , stability and crystallization *Proc. Earth Plan.*  
46 *Science*, **2014**, *10*, 143–148.
- 47 (45) Tlili, M. M.; Amor, M. B.; Gabrielli, C.; Joiret, S.; Maurin, G.; Rousseau, P. Characterization of CaCO<sub>3</sub>  
48 hydrates by micro-Raman spectroscopy *J. Raman Spectrosc.* **2001**, *33*, 10–16.
- 49 (46) Politi, B. Y.; Levi-Kalisman, Y.; Raz, S.; Wilt, F.; Addadi, L.; Weiner, S.; Sagi, I. Structural  
50 characterization of the transient amorphous calcium carbonate precursor phase in sea urchin embryos *Adv.*  
51 *Funct. Mater.* **2006**, *16*, 1289–1298.
- 52 (47) Herman, R. G.; Bogdan, C. E.; Sommer, A. J.; Simpson, D. R. Discrimination among carbonate minerals  
53 by Raman spectroscopy using the laser microprobe *Appl. Spectrosc.* **1987**, *41*, 437–440.
- 54 (48) Radha, A. V.; Fernandez-Martinez, A.; Hu, Y.; Jun, Y.-S.; Waychunas, G. A.; Navrotsky, A. Energetic  
55 and structural studies of amorphous Ca<sub>1-x</sub>Mg<sub>x</sub>CO<sub>3</sub>·nH<sub>2</sub>O (0≤x≤1) *Geochim. Cosmochim. Acta* **2012**, *90*, 83–95.
- 56 (49) Reeder, R. J.; Tang, Y.; Schmidt, M. P.; Kubista, L. M.; Cowan, D. F.; Philips, B. L. Characterization of  
57 structure in biogenic amorphous calcium carbonate: Pair distribution function and nuclear magnetic resonance  
58 studies of lobster gastrolith *Cryst. Growth Des.* **2013**, *13*, 1905–1914.
- 59 (50) Politi, Y.; Batchelor, D. R.; Zaslansky, P.; Chmelka, B. F.; Weaver, J. C.; Sagi, I.; Weiner, S.; Addadi, L.  
60 Role of magnesium ion in the stabilization of biogenic amorphous calcium carbonate: A structure - function  
61 investigation *Chem. Mater.* **2010**, *12*, 161–166.
- (51) Purgstaller, B.; Mavromatis, V.; Immenhauser, A.; Dietzel, M. Transformation of Mg-bearing amorphous

1  
2  
3 calcium carbonate to Mg-calcite – In situ monitoring *Geochim. Cosmochim. Acta* **2016**, *174*, 180–195.

4 (52) Boskey, A. L.; Posner, A. S. Conversion of amorphous calcium phosphate to microcrystalline  
5 hydroxyapatite *J. Phys. Chem.* **1973**, *77*, 2313–2317.

6 (53) Rodriguez-Blanco, J. D.; Shaw, S.; Bots, P.; Benning, L. G. The role of pH and Mg on the stability and  
7 crystallization of amorphous calcium carbonate *J. Alloys Compd.* **2012**, *536S*, S477-S479.

8 (54) Raz, B. S.; Hamilton, P. C.; Wilt, F. H.; Weiner, S.; Addadi, L. The transient phase of amorphous calcium  
9 carbonate in sea urchin larval spicules: The involvement of proteins and magnesium ions in its formation and  
10 stabilization *Adv. Funct. Mater.* **2003**, *13*, 480–486.

11 (55) Kim, Y.-Y.; Carloni, J. D.; Demarchi, B.; Sparks, D.; Reid, D. G.; Kunitake, M. E.; Tang, C. C.; Duer, M.  
12 J.; Freeman, C. L.; Pokroy, B.; Penkman, K.; Harding, J. H.; Estroff, L. A.; Baker, S. P.; Meldrum, F. C. Tuning  
13 hardness in calcite by incorporation of amino acids *Nat. Mater.* **2016**, *15*, 903-910.

14 (56) Von Euw, S.; Zhang, Q.; Manichev, V.; Murali, N.; Gross, J.; Feldman, L. C.; Gustafsson, T.; Flach, C.;  
15 Mendelsohn, R.; Falkowski, P. G. Biological control of aragonite formation in stony corals *Science* **2017**, *356*,  
16 933–938.

17 (57) Sevilgen, D. S.; Venn, A. A.; Hu, M. Y.; Tambutté, E.; de Beer, D.; Planas-Bielsa, V.; Tambutté, S. Full  
18 in vivo characterization of carbonate chemistry at the site of calcification in corals *Sci. Adv.* **2019**, *5*,  
19 doi:10.1126/sciadv.aau7447.

20 (58) Decarlo, T. M.; Comeau, S.; Cornwall, C. E.; McCulloch, M. T. Coral resistance to ocean acidification  
21 linked to increased calcium at the site of calcification *Proc. R. Soc. B Biol. Sci.* **2018**, *285*, 20180564.

22 (59) Decarlo, T. M. Characterizing coral skeleton mineralogy with Raman spectroscopy *Nat. Commun.* **2018**,  
23 *9*, doi:10.1038/s41467-018-07601-3.

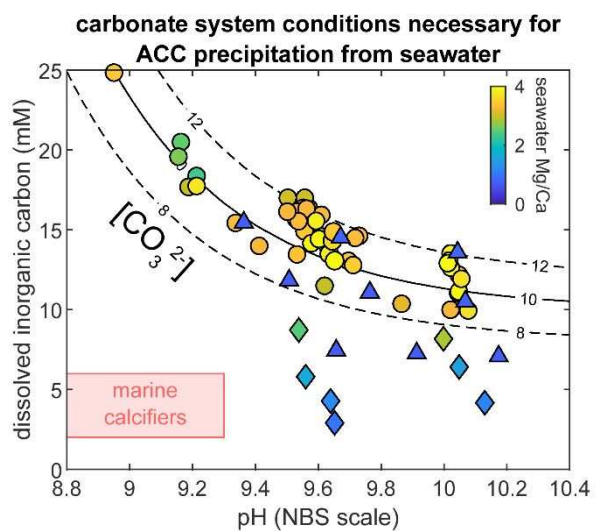
24 (60) Akiva, A.; Neder, M.; Kahil, K.; Gavriel, R.; Pinkas, I.; Goobes, G.; Mass, T. Minerals in the pre-settled  
25 coral *Stylophora pistillata* crystallize via protein and ion changes *Nat. Commun.* **2018**, *9*, doi:10.1038/s41467-  
26 018-04285-7.

27 (61) de Nooijer, L. J.; Spero, H. J.; Erez, J.; Bijma, J.; Reichart, G. J. Biomineralization in perforate  
28 foraminifera *Earth-Science Rev.* **2014**, *135*, 48–58.  
29  
30  
31  
32  
33  
34  
35  
36  
37  
38  
39  
40  
41  
42  
43  
44  
45  
46  
47  
48  
49  
50  
51  
52  
53  
54  
55  
56  
57  
58  
59  
60

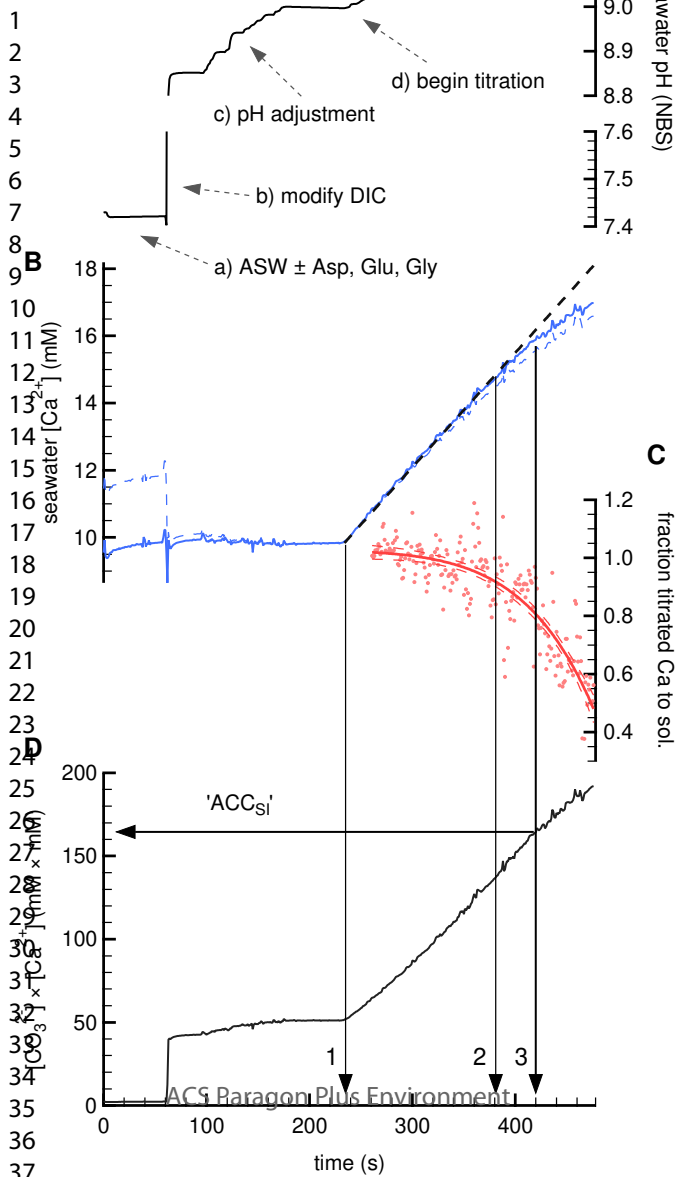


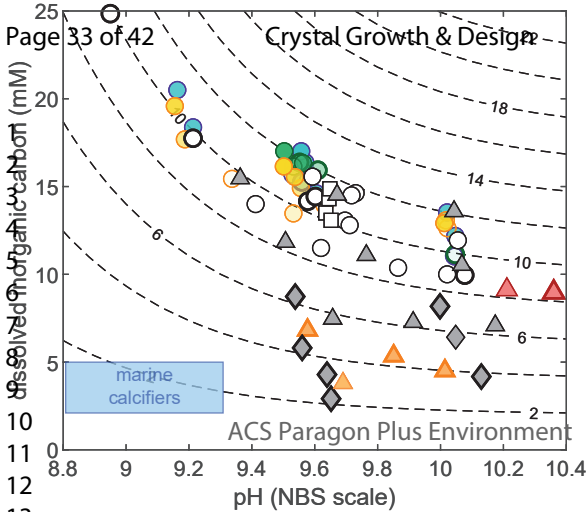
**For Table of Contents Use Only****The characteristics and biological relevance of inorganic amorphous calcium carbonate (ACC) precipitated from seawater**

David Evans, Paul B. Webb, Kirsty Penkman, Roland Kröger, and Nicola Allison

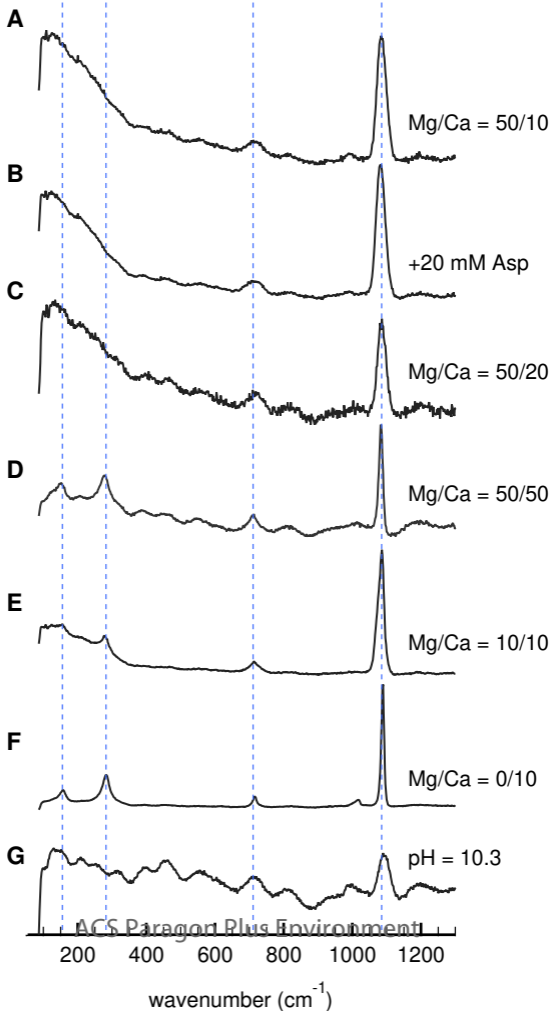


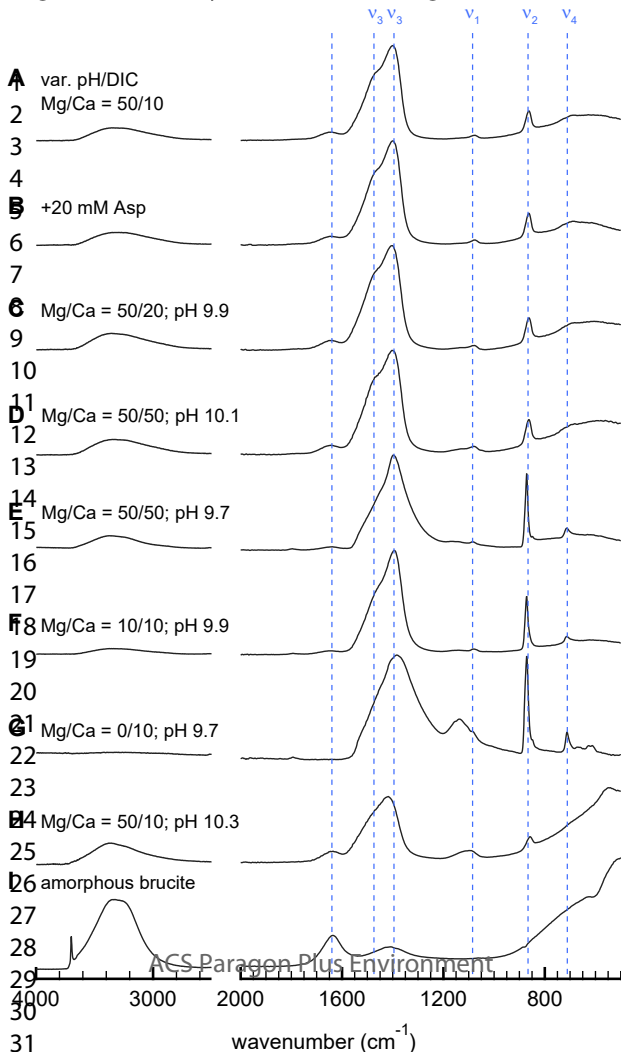
ACC precipitated from normal seawater is formed at a  $[CO_3^{2-}]$  of  $10 \pm 2$  mM, exceeding that at the calcification site of marine organisms reported to utilise an ACC precursor such as corals. The only investigated method of lowering the necessary [DIC] for precipitation was to reduce the seawater Mg/Ca ratio, raising the possibility that this is an important component of utilising an ACC pathway.

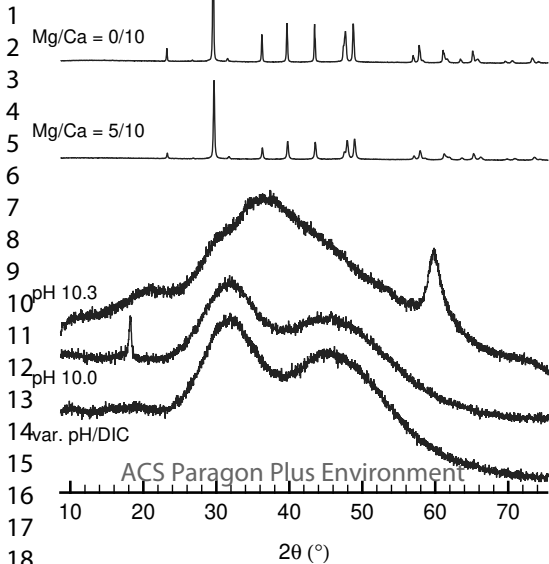


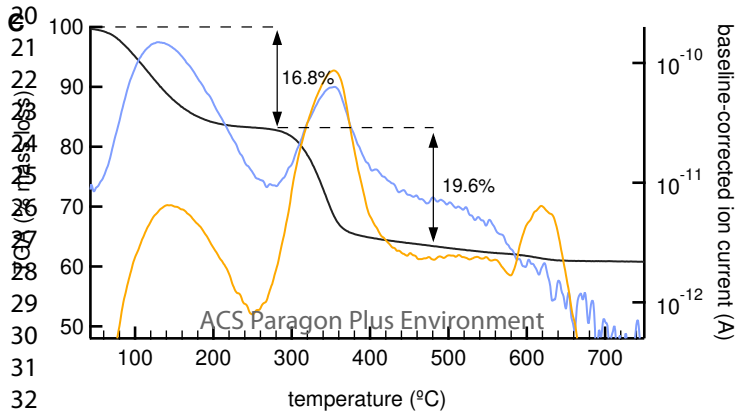
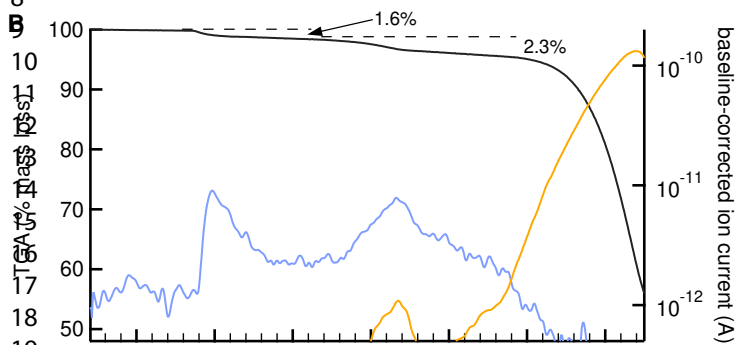
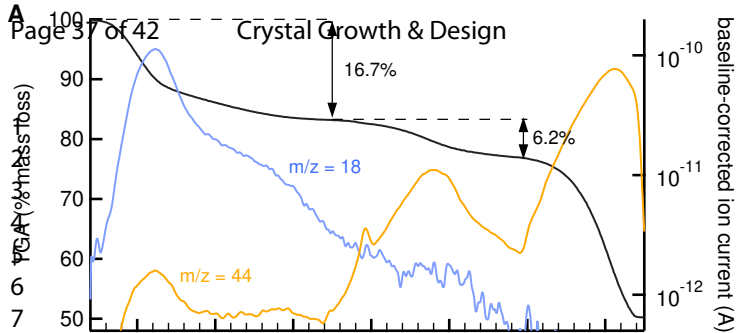


- Principal experimental variable:
- pH/DIC
  - Titration rate
  - ◇ Seawater [Ca]
  - [Asp]
  - [Glu]
  - [Gly]
  - △ pH/DIC@10 mM [Mg]
- Dominant precipitate of experiments that did not exclusively yield ACC:
- ▲ ACC/brucite
  - ▲ calcite

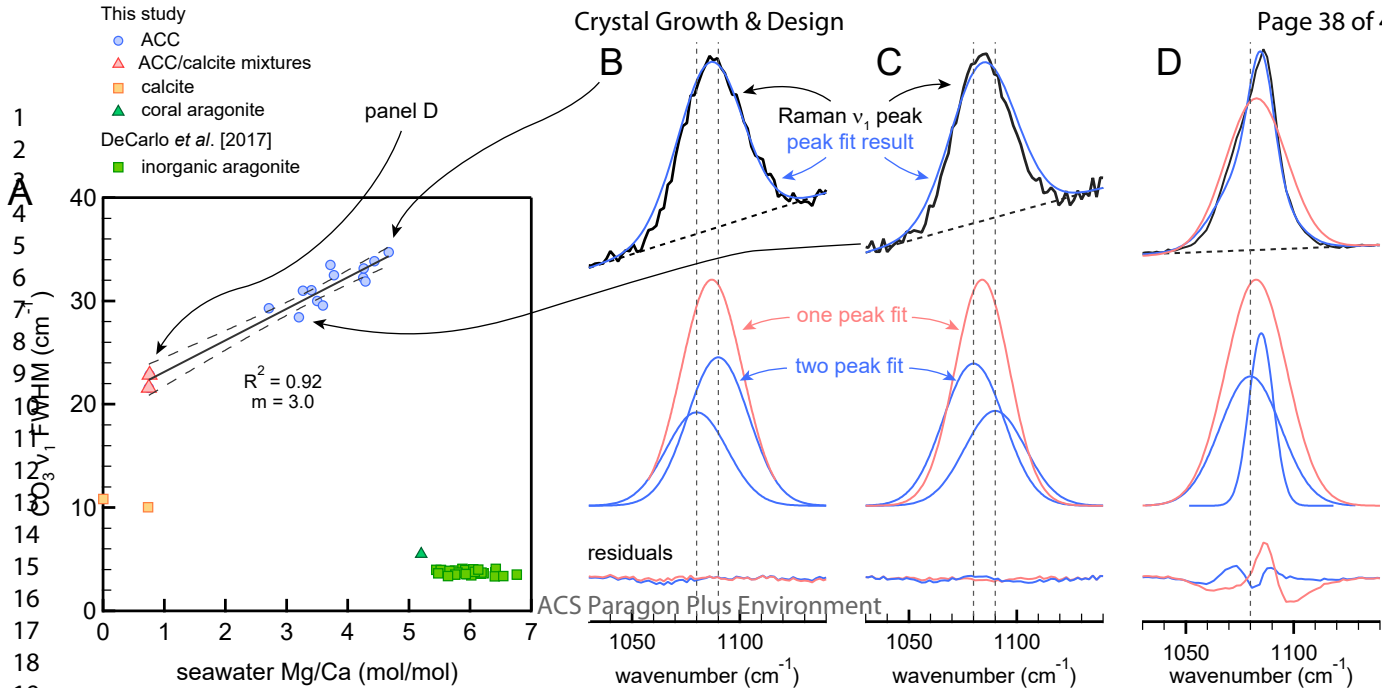




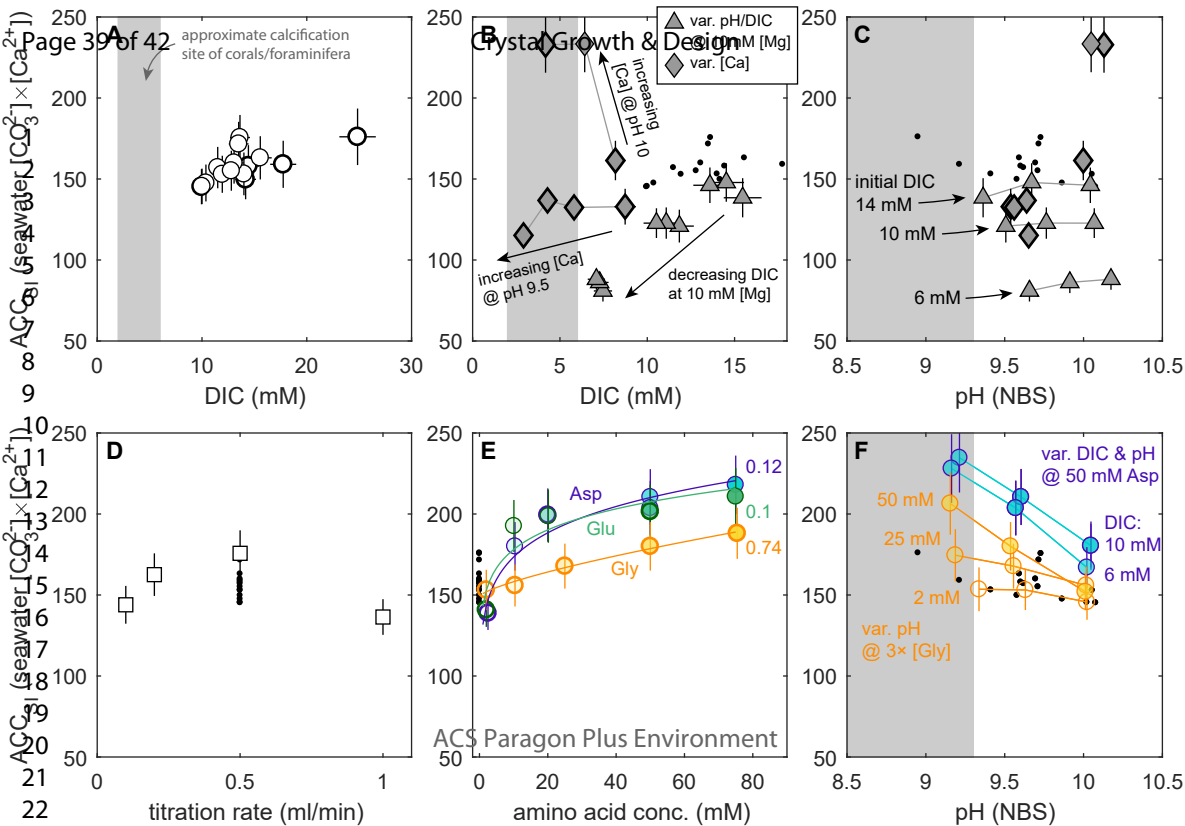


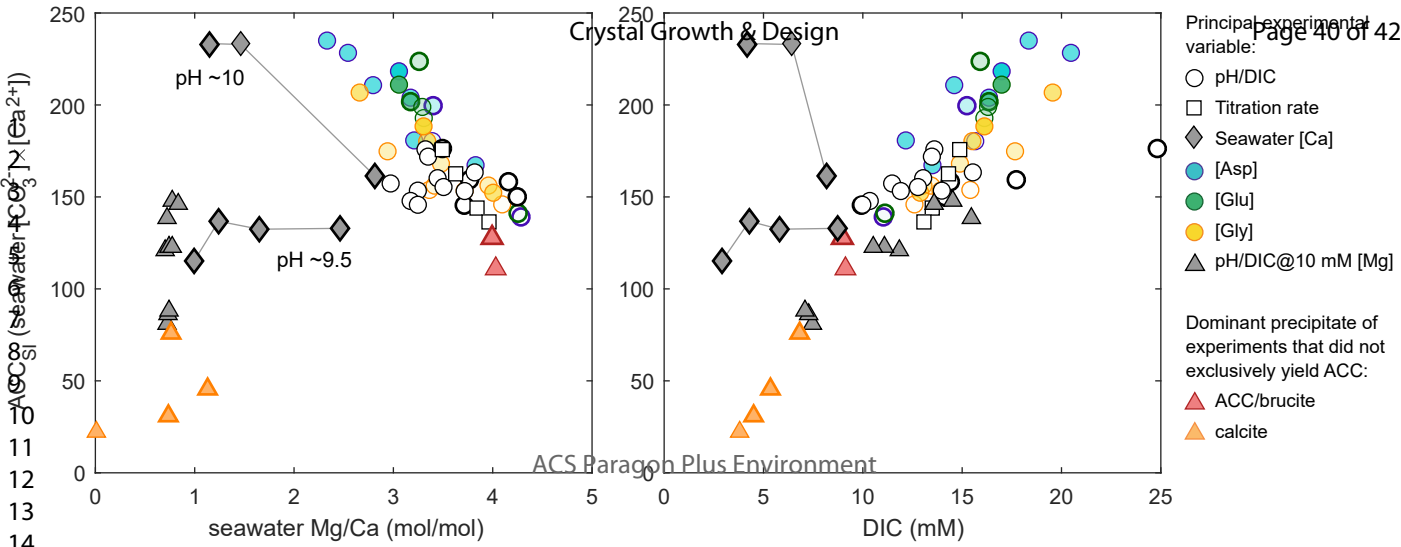


## Crystal Growth &amp; Design









11  
12  
13  
14

# Crystal Growth & Design

seawater Mg/Ca has a constant value  
 $[\text{CO}_3^{2-}]$  required to precipitate ACC

